

ORIGINAL ARTICLE

Endocytosis following dopamine D₂ receptor activation is critical for neuronal activity and dendritic spine formation via Rabex-5/PDGFR β signaling in striatopallidal medium spiny neurons

N Shioda¹, Y Yabuki², Y Wang³, M Uchigashima⁴, T Hikida⁵, T Sasaoka⁶, H Mori⁷, M Watanabe⁴, M Sasahara⁸ and K Fukunaga²

Aberrant dopamine D₂ receptor (D₂R) activity is associated with neuropsychiatric disorders, making those receptors targets for antipsychotic drugs. Here, we report that novel signaling through the intracellularly localized D₂R long isoform (D_{2L}R) elicits extracellular signal-regulated kinase (ERK) activation and dendritic spine formation through Rabex-5/platelet-derived growth factor receptor- β (PDGFR β)-mediated endocytosis in mouse striatum. We found that D_{2L}R directly binds to and activates Rabex-5, promoting early-endosome formation. Endosomes containing D_{2L}R and PDGFR β are then transported to the Golgi apparatus, where those complexes trigger Gai3-mediated ERK signaling. Loss of intracellular D_{2L}R-mediated ERK activation decreased neuronal activity and dendritic spine density in striatopallidal medium spiny neurons (MSNs). In addition, dendritic spine density in striatopallidal MSNs significantly increased following treatment of striatal slices from wild-type mice with quinpirole, a D₂R agonist, but those changes were lacking in D_{2L}R knockout mice. Moreover, intracellular D_{2L}R signaling mediated effects of a typical antipsychotic drug, haloperidol, in inducing catalepsy behavior. Taken together, intracellular D_{2L}R signaling through Rabex-5/PDGFR β is critical for ERK activation, dendritic spine formation and neuronal activity in striatopallidal MSNs of mice.

Molecular Psychiatry advance online publication, 6 December 2016; doi:10.1038/mp.2016.200

INTRODUCTION

The dopamine D₂ receptor (D₂R) is a member of the seven transmembrane and trimeric GTP-binding protein-coupled receptor family and, based on pharmacological properties, sequence homology and structure, specifically belongs to the D₂-like receptor subfamily (including D₂, D₃ and D₄).¹ D₂R is implicated in neurological and psychiatric diseases, and the abilities of antipsychotic drugs to block D₂R correlate with antipsychotic efficacy in clinical settings.² Genetic studies show significant association of *DRD2* polymorphisms with several disorders, including schizophrenia³ and Parkinson's disease.⁴ D₂R exists as two alternatively spliced isoforms, the D₂R long isoform (D_{2L}R) and the D₂R short isoform (D_{2S}R), which differ in a 29-amino-acid (AA) insert in the third cytoplasmic loop.⁵ D_{2L}R knockout (D_{2L}R-KO) mice display age-related deficits in motor and learning functions.⁶ Frequent intronic single-nucleotide polymorphisms (rs2283265 and rs1076560) decrease expression of D_{2S}R mRNA relative to D_{2L}R in human striatum and prefrontal cortex.⁷ Both intronic single-nucleotide polymorphisms are also associated with greater activity in the striatum and prefrontal cortex during working memory tasks, as measured using functional magnetic resonance imaging, an outcome associated with reduced performance in

working memory and attentional control tasks.⁷ This evidence indicates functional diversity between the two isoforms.

D₂R is coupled to pertussis toxin (PTX)-sensitive Gi/o proteins, and its activation can inhibit adenylyl cyclase, activate K⁺ channels, inhibit Ca²⁺ channels and stimulate Na⁺/H⁺ antiporters.⁸ Independent of conventional G protein pathways, activated D₂R induces formation of β -arrestin2/Akt/protein phosphatase 2A signaling complexes.⁹ D₂R stimulation also activates mitogen-activated protein kinase/extracellular signal-regulated kinase (ERK) in primary striatal neurons¹⁰ and brain slices.¹¹ ERK activation by D₂R stimulation is mediated by several signaling pathways including stimulation of Ras GTP-binding protein in C6 glioma cells¹² and G $\beta\gamma$ subunits of Gi/o proteins in Chinese hamster ovary cells.¹³ We previously reported that 40 AA residues in the D_{2L}R third cytoplasmic loop are essential for ERK activation in NG-108-15 cells.^{14,15} Transactivation of receptor tyrosine kinases such as platelet-derived growth factor receptor- β (PDGFR β) through activation of G_i (G α and/or G $\beta\gamma$) is also critical for D₂R-mediated ERK activation in Chinese hamster ovary cells.¹⁶ D₂R transactivation of PDGFR β inhibits *N*-methyl-D-aspartate-evoked currents in the hippocampus and prefrontal cortex in rats.^{17,18}

¹Department of Biofunctional Analysis Laboratory of Molecular Biology, Gifu Pharmaceutical University, Gifu, Japan; ²Department of Pharmacology, Graduate School of Pharmaceutical Sciences, Tohoku University, Sendai, Japan; ³Department of Pharmacology, Beckman Institute, University of Illinois, Urbana, IL, USA; ⁴Department of Anatomy, Hokkaido University Graduate School of Medicine, Sapporo, Japan; ⁵Department of Research and Drug Discovery, Medical Innovation Center, Kyoto University Graduate School of Medicine, Kyoto, Japan; ⁶Department of Comparative and Experimental Medicine, Brain Research Institute, Niigata University, Niigata, Japan; ⁷Department of Molecular Neuroscience, Graduate School of Medicine and Pharmaceutical Sciences, University of Toyama, Toyama, Japan and ⁸Department of Pathology, Graduate School of Medicine and Pharmaceutical Sciences for Research, University of Toyama, Toyama, Japan. Correspondence: Dr N Shioda, Department of Biofunctional Analysis Laboratory of Molecular Biology, Gifu Pharmaceutical University, 1-25-4 daigaku-nishi, Gifu 501-1196, Japan or Professor K Fukunaga, Department of Pharmacology, Graduate School of Pharmaceutical Sciences, Tohoku University, 6-3 Aramaki-Aoba, Aoba-ku, Sendai, Miyagi 980-8578, Japan.
E-mail: shioda@gifu-pu.ac.jp or kfukunaga@m.tohoku.ac.jp

Received 7 March 2016; revised 28 September 2016; accepted 4 October 2016

However, the physiological relevance of activation of ERK by D₂R through PDGFRβ has not been elucidated.

Here we report a novel mechanism underlying ERK activation through intracellular D₂L₁R signaling and reveal how that activity regulates synaptic function of striatopallidal medium spiny neurons (MSNs). We first identified that Rabex-5, which is a guanine nucleotide exchange factor (GEF) for Rab5,¹⁹ functions in intracellular D₂L₁R signaling. Rab5-dependent endocytosis through Rabex-5 activation elicited signaling through intracellular D₂L₁R together with PDGFRβ-mediated ERK activation. Moreover, novel intracellular D₂L₁R signaling through Rabex-5/PDGFRβ was critical for dendritic spine formation and neuronal activity in mouse striatopallidal MSNs.

MATERIALS AND METHODS

Animals

Mice were housed under climate-controlled conditions with a 12-h light/dark cycle and were provided standard food and water *ad libitum*. All animal procedures were approved by the Committee on Animal Experiments at Tohoku University and are based on the NIH guidelines. Adult 8- to 10-week-old male mice were used in all experiments. For conditional PDGFRβ deletion in the central nervous system, we crossed mice harboring PDGFRβ^{fl/fl} and with a line expressing Cre recombinase driven by the nestin promoter and enhancer as described.²⁰ D₂L₁R heterozygous (D₂L₁R-HT) mice²¹ were backcrossed to a C57BL/6J genetic background for more than six generations. D₂L₁R-KO, D₂L₁R-HT and D₂L₁R-wild-type (WT) mice were generated by mating D₂L₁R-HT mice. Mice lacking D₂R on a C57BL/6J background have been described.²²

Purification of proteins binding to the D₂L₁R 29AA motif and MALDI-TOF mass spectrometry

Preparation of proteins binding to the D₂L₁R 29AA sequence was performed using a glutathione S-transferase (GST) Protein Interaction Pull-Down Kit (Pierce; Thermo Fisher Scientific, Rockford, IL, USA) according to the manufacturer's instructions. GST and GST-29AA peptides were first prepared in *Escherichia coli* BL21 and then immobilized to glutathione affinity resin. Mouse brain tissues were lysed in buffer containing 50 mM Tris-HCl (pH 7.5), 0.5 M NaCl, 4 mM EDTA, 4 mM EGTA, 1 mM Na₃VO₄, 50 mM NaF, 1 mM dithiothreitol and protease inhibitors (trypsin, pepstatin A and leupeptin inhibitors), followed by centrifugation and incubation with immobilized glutathione affinity resin containing GST fusion proteins at 4 °C for 4 h with constant rotation. Subsequently, bound proteins were washed, eluted with glutathione elution buffer and run on sodium dodecylsulphate-polyacrylamide gel electrophoresis (SDS-PAGE). The gel was stained using a Silver Stain MS Kit (Wako, Osaka, Japan), and specific protein bands were excised. For protein identification by peptide mass fingerprinting, gel proteins were digested with trypsin (Promega, Madison, WI, USA), mixed with α-cyano-4-hydroxycinnamic acid (Sigma-Aldrich, St Louis, MO, USA) in 50% acetonitrile/0.1% trifluoroacetic acid, and were subjected to matrix-assisted laser desorption/ionization-time of flight (MALDI-TOF) analysis (Microflex LRF 20, Bruker Daltonics, Billerica, MA, USA). Spectra were collected from 300 shots per spectrum over an *m/z* range of 600–3000 and calibrated by two-point internal calibration using trypsin autodigestion peaks (*m/z* 842.5099, 2211.1046). A peak list was generated using Flex Analysis 3.0 (Bruker Daltonics). Thresholds used for peak-picking were as follows: 500 for minimum resolution of monoisotopic mass, 5 for S/N. The search program MASCOT, developed by Matrixscience (<http://www.matrixscience.com/>), was used for protein identification by peptide mass fingerprinting. The following parameters were used for the database search: trypsin as the cleaving enzyme, a maximum of one missed cleavage, iodoacetamide (Cys) as a complete modification, oxidation (Met) as a partial modification, monoisotopic masses and a mass tolerance of ±0.1 Da. Peptide mass fingerprinting acceptance criteria were probability-scoring.

Plasmid constructs and RNA interference

D₂L₁R-enhanced green fluorescent protein (EGFP) and D₂₅R-EGFP plasmids were prepared as described.^{14,15} The D₂L₁R GST-29AA motif was generated by cloning the D₂L₁R fragment into pGEX-4T-1. FLAG-D₂L₁R, FLAG-D₂₅R and HaloTag-PDGFRβ constructs (WT, ΔC, ΔC1, ΔC2, ΔC3 and KD) were

generated using the KOD-Plus Mutagenesis kit (Toyobo, Osaka, Japan) according to the manufacturer's protocol. Rabex-5, Rabex-5-D313A, Rabex-5C, Rabex-5C-D313A and Rabex-5 short hairpin RNA (shRNA) plasmids were kindly provided by Dr Mitsunori Fukuda (Tohoku University, Sendai, Japan).²³ His-tagged Rabex-5 were purified using Ni-NTA Sepharose (GE Healthcare, Piscataway, NJ, USA). Rab5(WT), Rab5(S34N) and Rab5(Q79L) plasmids were kindly provided by Dr Wei-Xing Zong (Stony Brook University, Stony Brook, NY, USA). GST-R5BD (the Rab5-binding domain residues 739–862 of Rabaptin-5-pGEX) was kindly provided by Dr Guangpu Li (University of Oklahoma Health Sciences Center, Oklahoma City, OK, USA). D₂L₁R-RLuc8, D₂₅R-RLuc8, Gai1-mVenus, Gai2-mVenus and Gai3-mVenus plasmids were kindly provided by Dr Jonathan A Javitch (Columbia University, New York, NY, USA). Gai3-C351G, which is a PTX-insensitive Gai3 mutant,²⁴ was generated using the KOD-Plus Mutagenesis kit (Toyobo). Rabex-5 short interfering RNA (siRNA; 5'-CAGAUAUCAUUGA GAUGGA-3'), Gai3 siRNA (5'-UCAAGGAACUCUACUCAA-3') and scrambled negative control siRNAs for each gene were purchased from Exigen (Tokyo, Japan). D₂R shRNA (TRCN0000025707), PDGFRβ shRNA (TRCN0000321931) and Gai3 shRNA (TRCN0000098262) were purchased from Sigma-Aldrich. The non-targeting hairpin control SHC002 (Sigma-Aldrich), containing a sequence that does not target any known human or mouse gene, was used as a negative control.

Cell culture and transfection

HEK293T cells were grown in Dulbecco's minimal essential medium supplemented with 10% heat-inactivated fetal bovine serum and penicillin/streptomycin (100 units per 100 μg ml⁻¹) in a 5% CO₂ incubator at 37 °C. Cells were transfected using Lipofectamine 2000 (Invitrogen, Carlsbad, CA, USA), and experiments were performed 48 h later as described.²⁵ For primary cultures, we used primary co-culture of striatal neurons with mesencephalic dopamine (DA) neurons to maintain intrinsic source of DA. Striatum and substantia nigra were dissected from embryonic day-18 mice, dissociated using trypsin, and triturated through a Pasteur pipette. Striatal neurons were transfected with expression vectors and/or shRNAs using electroporation (NEPA21; NEPAGENE, Chiba, Japan). Then, striatal neurons with mesencephalic neurons were plated on coverslips coated with poly-L-lysine in Minimum Essential Medium (Invitrogen) supplemented with 10% fetal bovine serum, 0.6% glucose (Wako) and 1 mM pyruvate (Sigma-Aldrich). After cell attachment, coverslips were transferred to a dish containing a glial cell monolayer and maintained in a Neurobasal medium (Invitrogen) containing 2% B27 supplement (Invitrogen) and 1% GlutaMax (Invitrogen). Cytosine β-D-arabinofuranoside (5 μM; Sigma-Aldrich) was added to cultures at day-*in vitro* (DIV)3 after plating to inhibit glial cell proliferation. When cells were treated with DA (Sigma-Aldrich), 0.02% ascorbic acid (Sigma-Aldrich) was added to DA-containing solution to prevent DA oxidation. For inhibitor analysis, cells were pre-incubated with haloperidol (Sigma-Aldrich), dynasore (Sigma-Aldrich), tyrphostin A9 (Sigma-Aldrich) or PTX (Sigma-Aldrich) for 1 h with the indicated concentrations.

Bioluminescence resonance energy transfer assay

Bioluminescence resonance energy transfer (BRET) was performed as described.²⁶ Briefly, HEK293T cells were seeded on 10 cm plates and transfected with plasmids encoding RLuc8-tagged D₂R isoforms, WT-PDGFRβ and mVenus-tagged Gai isoforms. At 48 h after transfection, cells were harvested, washed and suspended in phosphate-buffered saline (PBS). Approximately 200 000 cells per well were distributed to 96-well plates, and 5 μM coelenterazine H was added to each well. One minute later, DA was added to each well and fluorescence (excitation at 500 nm and emission at 540 nm, 1 s recording) and luminescence (no filters, 1 s recording) were immediately quantified using a Flexstation3 Multimode Plate Reader (Molecular Device, Sunnyvale, CA, USA). In parallel cells, the BRET signal was determined by quantifying and calculating the ratio of light emitted by mVenus (510–540 nm) to that emitted by RLuc8 (485 nm). BRET values were obtained by subtracting background in cells expressing RLuc8 alone.

Preparation of acute striatal slices

For slice preparations, acute 250 μm-thick coronal striatal brain slices were cut on a vibratome and allowed to recover for at least 1 h in continuously oxygenated (95% O₂ and 5% CO₂) artificial cerebrospinal fluid at 34 °C.

GST-R5BD pull-down assay

Assays were described previously.²⁷ Briefly, GST-R5BD was expressed in *E. coli* BL21 and purified using glutathione agarose beads. HEK293T cells and acute striatal slices were treated with 10 μ M quinpirole for 10 min. For pull-down assays, samples were lysed in buffer containing 50 mM Tris-HCl (pH 7.5), 0.5 M NaCl, 4 mM EDTA, 4 mM EGTA, 1 mM Na₂VO₄, 50 mM NaF, 1 mM dithiothreitol and protease inhibitors. After centrifugation, supernatants were incubated with GST-R5BD beads for 30 min at 4 °C on a rotating mixer, washed with lysis buffer, boiled in SDS sample buffer and subjected to western blotting.

Immunoprecipitation and immunoblotting analysis

Immunoprecipitation and immunoblotting analysis was performed as described.²⁵ HEK293T cells or striatal tissues were homogenized in buffer containing 50 mM Tris-HCl (pH 7.5), 0.5 M NaCl, 4 mM EDTA, 4 mM EGTA, 1 mM Na₂VO₄, 50 mM NaF, 1 mM dithiothreitol and protease inhibitors and treated with SDS buffer with or without boiling. For sucrose gradient fractionation, nuclei and unbroken cells were removed by centrifugation at 1600 *g* for 5 min at 4 °C. Resulting supernatants were loaded on a discontinuous sucrose gradient formed by layers of 30, 25, 20, 15, 10 and 5% sucrose (wt/vol) freshly prepared in homogenization buffer. Gradients were centrifuged at 100 000 *g* for 16 h at 4 °C. Nine fractions were collected from the top. Antibodies used included the following: mouse monoclonal anti-Rabex-5 (1:500, BD Biosciences, San Jose, CA, USA), anti-Rab5 (1:500, BD Biosciences), anti-GM130 antibody (1:500, BD Biosciences), anti-Na⁺/K⁺ ATPase α -1 (1:1000, Millipore, Bedford, MA, USA), anti-His antibody (Abcam, Cambridge, MA, USA) and anti- β -tubulin (1:5000, Sigma-Aldrich); rabbit polyclonal anti-GFP (Clontech, Mountain View, CA, USA), anti-D₂R (1:1000, Millipore), anti-HaloTag (1:1000, Promega), anti-ubiquitin (1:1000; Dako, Golstrup, Denmark), anti-phospho-(p)ERK (1:1000, Cell Signaling Technology, Beverly, MA, USA), anti-ERK (1:1000, Cell Signaling Technology), anti-PDGFR β (Tyr857; 1:1000, Cell Signaling Technology), anti-Rab17 (Abcam, Cambridge, MA, USA) and anti-Gai3 (Cosmo Bio, Tokyo, Japan), goat polyclonal anti-PDGFR β (1:500, Neuromics, Edina, MN, USA) and horseradish peroxidase-conjugated anti-T7 tag antibody (Novagen, Darmstadt, Germany).

Live cell imaging

HEK293T cells were transiently co-transfected with EGFP-tagged D₂R or D₂₅R and HaloTag-PDGFR β . Forty-eight hours later, the cells were sequentially labeled for 15 min at 37 °C with HaloTag tetramethylrhodamine (5 μ M) ligand. After labeling, cells were rinsed with fresh media for 15 min and then imaged following DA stimulation every 3 s for 40 min using a confocal laser scanning microscope (LSM700, Zeiss, Thornwood, NY, USA).

Behavioral tests

Catalepsy was evaluated as described.²⁵ Time spent in a cataleptic position was monitored by positioning the mouse so that both front paws rested on a 0.3 cm diameter steel rod (covered with non-slippery tape) 3.5 cm above a bench surface. The time during which each mouse maintained this position was recorded up to a maximum of 2 min. Mice were injected with haloperidol (Sigma-Aldrich) or SCH23390 (Sigma-Aldrich) four times (first vehicle alone and then three drug doses). Catalepsy was measured 1 h after haloperidol or SCH23390 administration in each test session. Two consecutive test sessions were separated by 2 h. To measure locomotor activity, mice housed individually in standard plastic cages were positioned in an automated open-field activity monitor using digital counters with an infrared sensor (DAS system, Neuroscience, Tokyo, Japan). Quinpirole (in 0.9% NaCl) was administered immediately before placing the animals in plastic cages, and locomotion was recorded during 30 min. Haloperidol dissolved in 5% dimethylsulphoxide with distilled water was administered intraperitoneal in a volume of 10 ml kg⁻¹. SCH23390 was dissolved in saline and administered subcutaneous in a volume of 10 ml kg⁻¹. The videotapes were scored by a trained observer blind to genotype and treatment.

Adeno-associated virus preparation and injection of adeno-associated virus vectors

pAAV-Rab5, pAAV-Rabex-5 and pAAV-Rab5-IRES-GFP constructs were constructed by cloning Rab5 or Rabex-5 complementary DNA (cDNA) into pAAV-MCS or pAAV-IRES-GFP vectors (Stratagene, La Jolla, CA, USA),

respectively. The same plasmid backbone with no cDNA or GFP cDNA was used as control constructs, termed adeno-associated virus (AAV)-Control or AAV-GFP, respectively. Viral particles were produced using the AAV2 Helper-Free System (Stratagene), according to the manufacturer's protocol, and titered by using an AAVpro Titration Kit (Takara Shuzo, Tokyo, Japan). For stereotaxic viral injections, the same titer (6.0 \times 10⁸ gc μ l⁻¹) and equal amounts (1 μ l) of viral particles were bilaterally injected into the striatum stereotaxically at the following coordinates (anterior, 0.9 mm; lateral, \pm 1.5 mm; depth, -3.0 mm relative to the bregma) through a Hamilton syringe (Hamilton Company, Reno, NV, USA). Four weeks later, the mice were analyzed behaviorally and immunohistochemically.

Immunohistochemistry and confocal microscopy

Immunohistochemistry was performed as described.²⁵ Primary antibodies included the following: mouse monoclonal anti-Rab5 (1:500, BD Biosciences), anti-GM130 (1:500, BD Biosciences), anti-TGN38 (1:500, BD Biosciences), anti-LAMP-1 (1:500, BD Biosciences), anti-endosomal autoantigen 1 (EEA1; 1:1000, BD Biosciences), anti-Cytochrome *c* (1:500, BD Biosciences), anti-synaptophysin (Syn; 1:1000, Sigma-Aldrich), anti-pERK (1:1000, Sigma-Aldrich), anti-FLAG (1:1000, Sigma-Aldrich) and anti-ryanodine receptor (1:1000, Millipore); rabbit polyclonal anti-GFP (1:000, Clontech), anti-D₁R (1:1000, Millipore), anti-D₂R (1:1000, Millipore), anti-tyrosine hydroxylase (1:1000, Millipore), anti-HaloTag (1:1000, Promega), anti-DARRP-32 (1:1000, Millipore) and anti-preproenkephalin (ppEnk; 1:1000, Neuromics); goat polyclonal anti-PDGFR β (1:500, Neuromics); and guinea pig polyclonal anti-VGLUT1 (1:1000, Millipore). Secondary antibodies included the following: Alexa 594-labeled anti-mouse IgG, Alexa 448 or Alexa 405-labeled anti-rabbit IgG (1:500, Invitrogen). Double-staining with PDGFR β and various marker (DARRP-32, D₁R, D₂R, VGLUT1 or tyrosine hydroxylase) antibodies was performed using biotinylated donkey anti-goat IgG (1:500; Jackson ImmunoResearch, West Grove, PA, USA) with a mixture of streptavidin-horseradish peroxidase (1:500, NEN Life Science Products, Boston, MA, USA) and Alexa 594 anti-rabbit or guinea pig IgG (1:500, Invitrogen). Finally, sections were stained with fluorescein tyramide for 10 min using a TSA-Direct kit (NEN Life Science Products). To detect ppEnk-positive cells, coronal brain sections were processed for antigen retrieval in 10 mM citrate buffer (0.05% Tween20, pH 6) and heated at 75 °C for 15 min. No staining was confirmed in the negative controls obtained by replacing the primary antibodies with isotype control primary IgGs. Sections were mounted in Vectashield (Vector Laboratories, Burlingame, CA, USA), and immunofluorescence was analyzed using a confocal laser scanning microscope (LSM700, Zeiss). Co-localization of organelles was quantified using the co-localization coefficient of Manders *et al.*²⁸ To quantify co-localization with the early-endosome marker EEA1, at least 5 μ m squares were randomly delineated in the cytosol and perinuclear region, and the number of EEA1-positive endosomes and structures labeled by both D₂R and PDGFR β within squares was determined. Endosomes containing both proteins were counted and reported as a percentage of EEA1-positive compartments. pERK and ppEnk double-positive cells were counted in four areas (350 \times 350 μ m per area) per section of the dorsal striatum (four sections per mouse, four mice per condition). The positions of dorsal striatum were indicated in Figure 1c of Shioda *et al.*²⁵

Proximity ligation *in situ* assay

A proximity ligation *in situ* assay (PLA) was performed using mouse striatal slices fixed in 4% paraformaldehyde (PFA) using the Duolink Detection Kit (Olink Bioscience, Uppsala, Sweden) according to the manufacturer's instructions. To detect interaction of PDGFR β with D₁R or D₂R, striatal slices were labeled with anti-goat Duolink PLA PLUS and anti-rabbit MINUS probes in a humidified oven at 37 °C using goat polyclonal anti-PDGFR β antibody (1:500, Neuromics) with rabbit polyclonal anti-D₁R antibody (1:1000, Millipore) or rabbit polyclonal anti-D₂R antibody (1:1000, Millipore). Oligonucleotide tails of secondary PLA PLUS and MINUS antibody probes hybridize when primary antibodies are in close proximity. Amplified end products appear as green fluorescent spots in imaging. Each green spot represents an interaction between protein molecules.

Lucifer yellow labeling of slice neurons

Intracellular lucifer yellow (LY) labeling methods were performed as described with minor modifications.^{20,29} To detect striatopallidal MSNs, fixed striatal slices were pre-stained with ppEnk and 4,6-diamidino-2-phenylindole (DAPI). As LY, ppEnk and DAPI fluorescence can be visualized simultaneously under ultraviolet excitation using a fluorescein long-pass

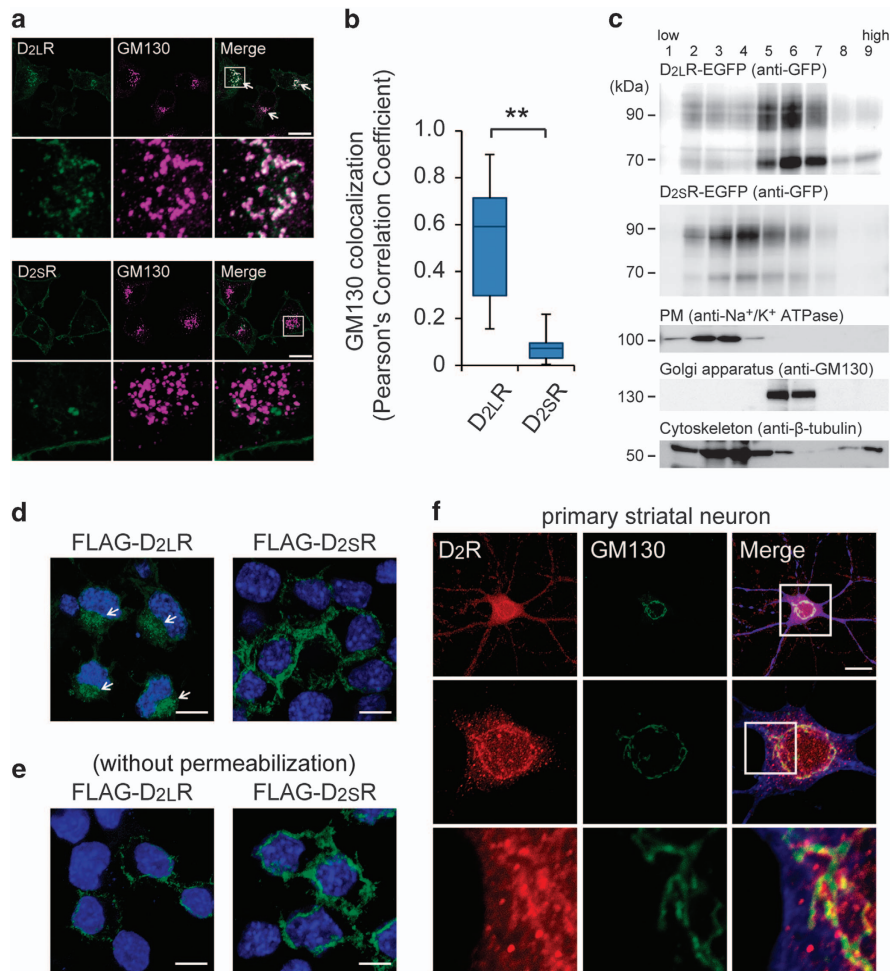


Figure 2. Localization of D₂ receptor (D₂R) long isoform (D₂L_R) in the Golgi complex. **(a)** Confocal images showing co-localization of EGFP-tagged D₂R isoforms with GM130, a cis-Golgi marker. Lower panels are high-magnification images of upper white rectangles. Scale bars, 10 μ m. **(b)** Pearson's correlation coefficients showed the co-localization of D₂R-EGFP isoforms with GM130. A total of 16 cells from three experiments were analyzed. ****** $P < 0.01$ by one-way analysis of variance (ANOVA) with *post hoc* Tukey test. **(c)** HEK293T cells expressing EGFP-tagged D₂R isoforms were fractionated on discontinuous sucrose-density gradients. Equal volumes from each fraction were separated by sodium dodecylsulphate-polyacrylamide gel electrophoresis (SDS-PAGE), followed by immunoblotting with indicated antibodies. Immunoblots were repeated three times and representative data are shown. PM, plasma membrane. **(d)** FLAG-D₂L_R- and FLAG-D₂S_R-expressing cells were immunostained with anti-FLAG antibody. Arrows indicate FLAG-tagged D₂L_R in the perinuclear region. **(e)** Cell surface expression of FLAG-tagged D₂R in FLAG-D₂L_R- and FLAG-D₂S_R-expressing cells as detected by immunostaining with the anti-FLAG antibody without cell permeabilization. Scale bars, 10 μ m. **(f)** Striatal neuron was triple-stained for anti-D₂R (red), anti-GM130 (green) and anti-MAP2 (blue). Scale bar, 10 μ m.

filter, we injected LY into specific striatopallidal MSNs. Sections were then fixed in 4% PFA in 0.1 m phosphate buffer, pH 7.4, for 24 h, washed several times with PBS, incubated 1 h in PBS containing with 1% bovine serum albumin, 0.3% Triton X-100 and 0.1% NaN₃ (as blocking solution), and then reacted with a rabbit anti-LY polyclonal antibody (1:5000, Invitrogen) in blocking solution at 20 $^{\circ}$ C for 5 days. After washing, sections were incubated three more days with Alexa 488-labeled anti-rabbit IgG (1:500, Invitrogen). After several washes in PBS, sections were mounted on slides. Immunofluorescent images were analyzed using a confocal laser scanning microscope (LSM700, Zeiss).

Analysis of spine morphology

Images were analyzed in using the ImageJ (NIH, Bethesda, MD, USA) software. Dendritic spine density was measured by counting the number of spines on secondary dendrite and reported as the number of spines per 20 μ m of dendrite length. Spine length was calculated as the radial distance from the tip of the spine head to the dendritic shaft. For branching analysis, dendrite morphology was quantified using the Sholl Analysis plugin of the ImageJ software.

Electrophysiology

For whole-cell patch clamp recording, spontaneous excitatory postsynaptic currents (sEPSCs) were recorded at room temperature (22–25 $^{\circ}$ C) on EGFP-expressing primary neurons derived from the striatum on DIV21 using an EPC10 amplifier (HEKA, Lambrecht/Pfalz, Germany). The following buffer was used (in mM): extracellular, 143 NaCl, 5 KCl, 2 CaCl₂, 1 MgCl₂, 10 glucose, 10 HEPES, pH 7.4 with NaOH; intracellular, 135 CsMeS, 5 CsCl, 10 HEPES, 0.5 EGTA, 1 MgCl₂, 4 Mg₂ATP, 0.4 NaGTP, 5 QX-314, pH 7.4 with CsOH. Recording pipettes made of borosilicate glass (B150-86-10; Sutter Instrument, Novato, CA, USA) had a resistance of 3.5–4.5 M Ω when filled with intracellular solution. sEPSCs were recorded for 2 min (1 min after break-in to block sodium current by QX-314) at holding potential –70 mV in the presence of 20 μ M bicuculline in extracellular solutions to block GABA_A receptors. Recordings were filtered at 2 kHz and digitized at 10 kHz. Access resistances were monitored throughout the experiment (< 15 M Ω) but not compensated. Data were collected and initially analyzed with the Patchmaster software (HEKA). Further analysis was performed using IgorPRO ver6.3 (Wavemetrics, Portland, OR, USA) and Excel (Microsoft, Redmond, WA, USA) and MiniAnalysis programs ver6.0.7.

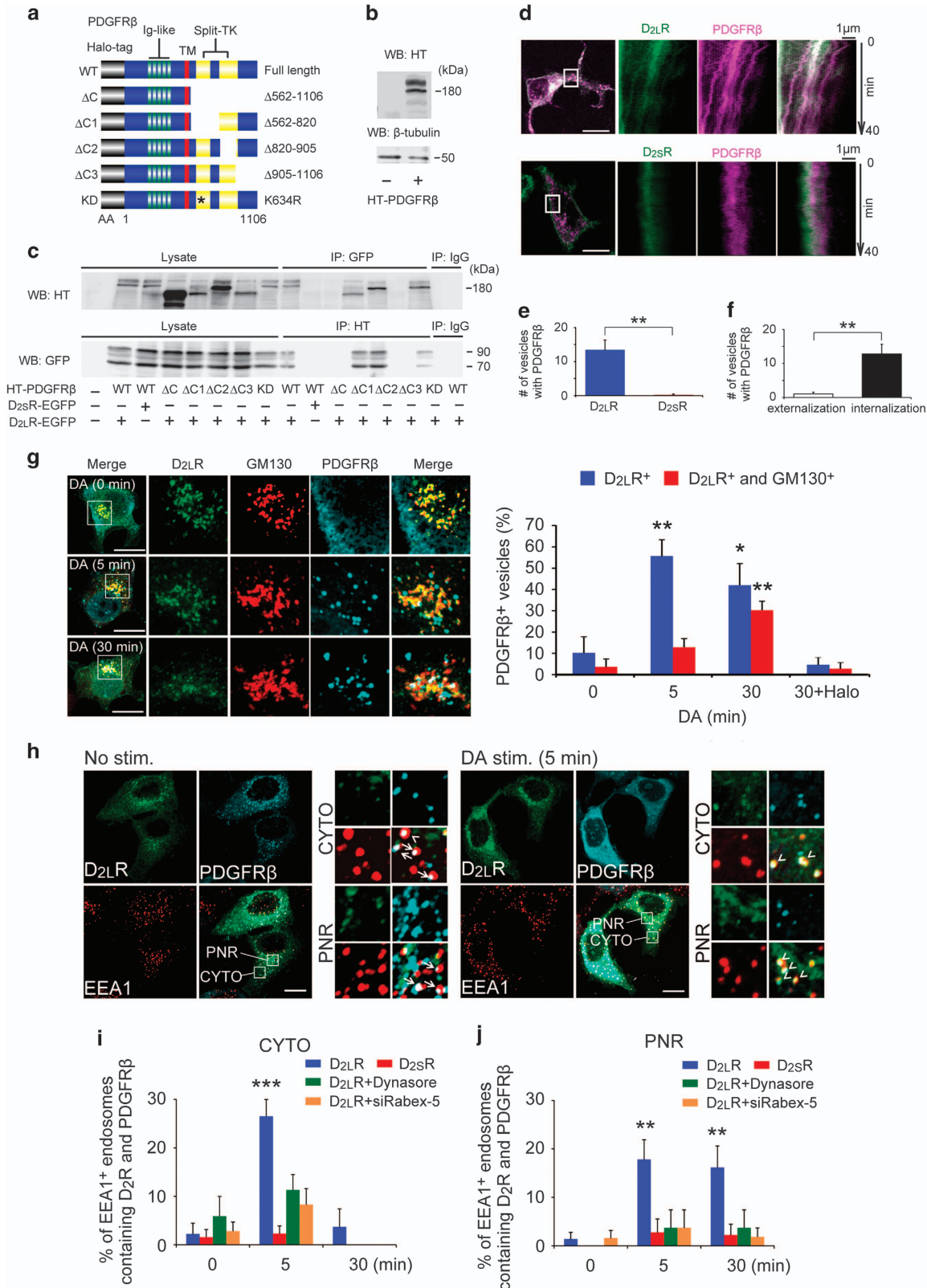
Statistical analysis

Statistical significance for differences among groups was tested by one-way or two-way analysis of variance (ANOVA) with *post hoc* Tukey tests. *P* < 0.05 was considered significant. All values (except for box-and-whisker plot) were presented as mean ± s.e.m.

RESULTS

Rabex-5 is a D₂L_R-interacting protein

As a first step in our search for novel mediators of D₂L_R signaling, we used the online I-TASSER software³⁰ to predict the



three-dimensional structure of human D_{2L}R protein. This analysis revealed that the 29AA insert found in D_{2L}R relative to the shorter form contains highly hydrophilic sequences exhibiting primarily an alpha-helical structure (Figure 1a). BLAST searches indicated conservation of this region in vertebrates from zebrafish to mammals, although the region was not conserved in invertebrates. To identify proteins binding to this motif, we performed pull-down assays in mouse brain lysates with GST-tagged peptides representing the 29AA sequence and observed several potential interactors following silver staining. Mass spectrometric analysis revealed that one was Rabex-5 (Rab5-GDP/GTP exchange factor; Figure 1b and Supplementary Figure 1). That direct interaction was confirmed by a GST-29AA pull-down assay in mouse brain lysates and in purified His-Rabex-5 protein (Figure 1c).

Rabex-5 is a Rabaptin-5 interacting protein, and the Rabex-5/Rabaptin-5 complex catalyzes nucleotide exchange for Rab5 and cooperates with other factors to promote endosome fusion.¹⁹ Rabex-5 exhibits an A20-like zinc-finger domain with ubiquitin ligase activity,^{31,32} a VPS9 domain comprising the GEF catalytic core,³³ and a C-terminal coiled-coil (CC) domain containing the Rabaptin-5-binding site.³⁴ To identify the region mediating D_{2L}R/Rabex-5 complex formation, we expressed EGFP-tagged D_{2L}R in HEK293T cells with four different T7-tagged Rabex-5 constructs: full-length, wild-type Rabex-5; a GEF activity-deficient mutant (Rabex-5-D313A);³³ the C terminus only containing the VPS9 domain (Rabex-5C); and the C terminus containing a mutant VPS9 domain lacking GEF activity (Rabex-5C-D313A; Figure 1d). After immunoprecipitation with EGFP-tagged D_{2L}R, T7-tagged Rabex-5 and Rabex-5C, but not Rabex-5-D313A or Rabex-5C-D313A, interacted with D_{2L}R-EGFP. When EGFP-tagged D₂₅R was coexpressed with T7-tagged Rabex-5, the interaction was lost (Figure 1e). Thus, the D_{2L}R 29AA interacts with Rabex-5 residues 208–491, a region that contains the VPS9 and CC domains and regulates GEF activity.

To confirm the interaction *in vivo*, we performed immunoprecipitation of striatal extracts with an anti-D₂R antibody followed by immunoblotting with anti-Rabex-5 antibody. Rabex-5 signals were present in striatal extracts from WT mice but not from D_{2L}R-KO or D₂R-KO mice. Conversely, after Rabex-5 immunoprecipitation from striatal extracts, immunoblotting with the anti-D₂R antibody detected D₂R in extracts of brain from WT but not D_{2L}R-KO or D₂R-KO mice (Figure 1f).

D_{2L}R/Rabex-5 complex formation may facilitate Rab5 activation by D_{2L}R signaling. To assess potential Rab5 activation following D₂R stimulation, we performed a pull-down assay using the GST-tagged Rab5-binding domain of Rabaptin-5 (R5BD), which binds to Rab5-GTP.²⁷ When cells were treated for 10 min with the D₂R agonist quinpirole, Rab5-GTP levels markedly increased in lysates of HEK293T cells coexpressing Rab5 (WT) and D_{2L}R (lane 6) compared with Rab5 (WT) alone (lane 2), and the increased Rab5-GTP levels were blocked by haloperidol (lane 8). GST-R5BD-binding specificity for active Rab5 was verified by the observation that Rab5-GTP levels are equivalent in coexpressing D_{2L}R and Rab5 (Q79L; constitutively active)-transfected cells with or without quinpirole (lanes 9 and 10), and did not increase Rab5-GTP levels in cells coexpressing D_{2L}R and Rab5 (S34N; dominant-negative) with quinpirole (lanes 11 and 12). Furthermore, Rab5-GTP levels in cells coexpressing D_{2L}R and a Rabex-5-D313A mutant were not upregulated following quinpirole treatment (lane 14; Figure 1g). Quinpirole treatment also significantly increased Rab5-GTP levels in striatal slices from WT mice but not in slices from D_{2L}R-KO mice (Figure 1h). We conclude that D_{2L}R signaling activates Rab5 through direct D_{2L}R/Rabex-5 interaction.

D_{2L}R is located in the plasma membrane and intracellular compartment

To determine D_{2L}R's subcellular localization, we performed analysis in HEK293T cells transfected with D_{2L}R-EGFP. We detected D_{2L}R-EGFP in the plasma membrane and perinuclear region, where intracellular D_{2L}R predominantly co-localized with the cis-Golgi marker GM130. D₂₅R-EGFP, by contrast, was mainly detected on the plasma membrane (Figure 2a). The Pearson correlation coefficients for D_{2L}R-EGFP and GM130 are significantly higher than those for D₂₅R-EGFP and GM130 (Figure 2b). D_{2L}R-EGFP and D₂₅R-EGFP did not co-localize with other organelle markers, such as markers of the endoplasmic reticulum (ryanodine receptor), mitochondria (cytochrome C) or the trans-Golgi-network (TGN38; Supplementary Figure 2a–g). Sucrose-density gradient fractionation confirmed D_{2L}R and D₂₅R localization. D_{2L}R-EGFP fractions peaked at fractions 5 and 6, coincident with the cis-Golgi marker GM130, whereas D₂₅R-EGFP fractions peaked at the plasma membrane fraction, as marked by Na⁺/K⁺ ATPase (Figure 2c). To examine whether HEK293T cells express equivalent protein levels of D₂R isoforms, we performed immunoblot analysis and counted GFP-positive cells after transfection with EGFP-tagged D₂R

Figure 3. D₂ receptor (D₂R) long isoform (D_{2L}R)/platelet-derived growth factor receptor-β (PDGFRβ) double-positive endosomes converge on Golgi complexes through clathrin-mediated endocytosis. **(a)** Schematic representation of PDGFRβ constructs. AA, amino acids. **(b)** HEK293T cells were transfected with wild type (WT) Halo-tagged (HT)-PDGFRβ construct. Western blots were probed with indicated antibodies. **(c)** HEK293T cells were co-transfected with D₂R-EGFP isoforms and indicated HT-PDGFRβ constructs. Cell lysates were immunoprecipitated with anti-GFP or anti-HT antibodies. Western blots (WBs) were probed with anti-HT or anti-GFP antibodies. **(d)** Time-lapse imaging of HEK293T cells co-transfected with EGFP-tagged D₂R isoforms (green)/tetramethylrhodamine (TMR)-labeled HT-PDGFRβ (magenta) following 10 μM DA stimulation. Left panels show first images of the series. White rectangle corresponds to the region used to create the kymograph. Right panels show representative kymographs and pseudocolor overlay of the two kymographs. **(e)** Quantification of D₂R isoforms and PDGFRβ double-positive vesicles. Most D_{2L}R-positive particles co-transport PDGFRβ as compared with D₂₅R. *n* = 9 cells for each group, three experiments were analyzed. (***P* < 0.01 by one-way analysis of variance (ANOVA) with *post hoc* Tukey test). **(f)** Quantification of externalized or internalized vesicles in D_{2L}R/PDGFRβ-co-transfected cells. Most D_{2L}R/PDGFRβ double-positive particles are endocytosed. Cells were pretreated with 10 μM haloperidol before addition of DA for 1 h. *n* = 9 cells for each group, three experiments were analyzed. (***P* < 0.01 by one-way ANOVA with *post hoc* Tukey test). **(g)** Triple-labeling immunofluorescence microscopy of D_{2L}R-EGFP (green), HT-PDGFRβ (cyan) and GM130 (red) with or without 10 μM DA in HEK293T cells. Images at bottom are enlarged from corresponding boxed areas. Quantitative analysis at lower right shows the percentage of D_{2L}R/PDGFRβ double-positive vesicles per the total number of PDGFRβ-positive vesicles (blue bars) or the percentage of D_{2L}R/PDGFRβ/GM130 triple-positive vesicles per total number of PDGFRβ-positive vesicles (red bars). ***P* < 0.01, **P* < 0.05 by two-way ANOVA with *post hoc* Tukey test. Nine fields (three cells per field) per condition were chosen randomly. Halo: haloperidol. **(h)** Triple-labeling immunofluorescence microscopy of D_{2L}R-EGFP (green), HT-PDGFRβ (cyan) and endosomal autoantigen 1 (EEA1; red) in cytosol (CYTO) and perinuclear region (PNR) with no stimulation (left) or with 10 μM DA for 5 min (right) in HEK293T cells. Boxed areas are enlarged at right. Arrows indicate PDGFRβ/EEA1 double-positive endosomes; arrowheads show D_{2L}R/PDGFRβ/EEA1 triple-positive endosomes. **(i, j)** Calculation of the percentage of D_{2L}R/PDGFRβ/EEA1 triple-positive endosomes per total EEA1-positive endosomes in CYTO and PNR. ****P* < 0.001, ***P* < 0.01 by two-way ANOVA with *post hoc* Tukey test. Nine fields per condition were chosen randomly for analysis (three cells per field). Scale bars, 10 μm.

isoforms. There was no statistical difference in the expression levels of EGFP-tagged D₂R isoforms in HEK293T cells (Supplementary Figure 2h and i). To confirm that these findings were not an artifact due to tagging with EGFP, we fused the lower molecular weight FLAG-tag to the N termini of D_{2L}R and D_{2S}R. Similar to the EGFP-tagged proteins, FLAG-tagged D_{2L}R was predominantly localized in the perinuclear region (Figure 2d, arrows) but weakly observed in the plasma membrane region, whereas D_{2S}R was predominantly localized at the plasma membrane region, as reported in NG-108-15 cells.³⁵ To detect cell surface D₂R expression, D_{2L}R FLAG-tagged at the extracellular N terminal was immunostained with an anti-FLAG antibody without cell permeabilization by Triton X-100. FLAG-D_{2L}R was not seen in intracellular compartments of FLAG-D_{2L}R-expressing cells and faintly seen in the plasma membranes (Figure 2e). To take into account possibility that HEK293T cells may lack the important chaperones required for D_{2L}R protein folding, we immunostained with anti-D₂R antibody in mouse primary striatal neurons. Immunocytochemical analysis revealed that D₂R is localized both in the plasma membrane and in the intracellular region, where it partly co-localized with GM130 in an intracellular compartment of MAP2-positive striatal neuron (Figure 2f). There was no background immunofluorescence without primary antibody as negative control (data not shown). Overall, D_{2L}R and D_{2S}R proteins were expressed at the plasma membrane, and D_{2L}R was also located intracellularly.

D_{2L}R is transported to the Golgi complex with PDGFR β by Rabex-5/Rab5-mediated endocytosis

Plasma membrane proteins can be internalized by endocytosis and transported to endosomes and Golgi apparatus.³⁶ In addition, based on reports that D₂R stimulation results in PDGFR β transactivation to promote inactivation of *N*-methyl-D-aspartate receptor in rat hippocampus and prefrontal cortex,^{17,18} we hypothesized that PDGFR β transactivation has a crucial role in D₂R signaling. To confirm the D_{2L}R/PDGFR β complex, we expressed EGFP-tagged D₂R isoforms in HEK293T cells with four different HaloTag (HT)-PDGFR β constructs (Figure 3a). To reveal the immunoreactive band of HT-PDGFR β , we performed immunoblot analysis with or without full-length HT-PDGFR β transfection using an anti-HT antibody in HEK293T cells (Figure 3b). Co-immunoprecipitation assays with D_{2L}R-EGFP in HEK293T cells revealed that the HT-PDGFR β C-terminal intracellular domain (AA905-1106) interacts with D_{2L}R (Figure 3c). We next visualized trafficking of these proteins in living cells co-transfected with D_{2L}R-EGFP and HT-PDGFR β labeled with tetramethylrhodamine. Data gathered from time-lapse movies (Supplementary Movies 1 and 2), kymographs (Figure 3d) and quantitative analysis indicated that the number of vesicles showing D₂R co-localization with PDGFR β was significantly greater in the presence of D_{2L}R than that with D_{2S}R (Figure 3e). D_{2L}R- and PDGFR β -containing vesicles exhibited endocytotic properties and moved in a retrograde direction (Figure 3f). When we analyzed D_{2L}R- and PDGFR β -containing vesicles in the soma, we observed that they accumulated significantly in the perinuclear region following DA stimulation, often in complexes positive for the GM130 (Figure 3g), suggesting that D_{2L}R interacts with PDGFR β , and the complex at the plasma membrane transported to endosomes and accumulated Golgi apparatus following DA stimulation.

We next focused on early-endosome formation, as increased Rab5-GTP levels due to D_{2L}R/Rabex-5 pathway activation may promote endocytosis. Endocytosis can be identified by recruitment of membrane-docking molecules such as EEA1.³⁷ Thus, we incubated HEK293T cells with or without DA after co-transfecting them with D_{2L}R-EGFP and HT-PDGFR β , and then stained cells with an anti-EEA1 antibody. When we assessed D_{2L}R-EGFP/HT-PDGFR β staining in cytoplasmic and perinuclear regions in fixed cells not

treated with DA, we found that most PDGFR β -positive vesicles co-localized with EEA1-positive endosomes (Figure 3h, arrows), whereas D_{2L}R and PDGFR β double-positive vesicles did not (< 2% of EEA1-positive endosomes). Following 5 min of DA treatment, however, we observed that a significant population of D_{2L}R/PDGFR β double-positive vesicles overlapped with EEA1-positive endosomes (20–30% of EEA1-positive endosomes in both cytosolic and perinuclear regions). After 30 min of DA stimulation, only 5% of EEA1-positive endosomes co-localized with D_{2L}R/PDGFR β double-positive vesicles in cytosolic regions. By contrast, in perinuclear regions, 20% of EEA1-positive endosomes co-localized with D_{2L}R/PDGFR β double-positive vesicles (Figure 3h, arrowheads) even at 30 min of DA treatment (Figure 3h–j). On the other hand, in cells co-transfected with D_{2S}R-EGFP and HT-PDGFR β , most D_{2S}R-labeled vesicles did not co-localize with EEA1-positive endosomes with or without DA treatment (< 3% of EEA1-positive endosomes). Pre-incubation of cells with the dynamin inhibitor dynasore, which blocks clathrin-mediated endocytosis, abolished DA-induced overlap of EEA1-positive endosomes with D_{2L}R/PDGFR β double-positive vesicles. Similar results were obtained when cells were transfected with Rabex-5 siRNA (Figure 3i and j). We confirmed siRNA efficacy on knockdown of Rabex-5 by immunoblotting of endogenous Rabex-5 protein in HEK293T cells (Supplementary Figure 3a). In addition, EEA1-positive endosomes with D_{2L}R/PDGFR β double-positive vesicles were significantly decreased by haloperidol (data not shown). These data suggest that DA treatment promotes transport of early endosomes containing D_{2L}R and PDGFR β to the Golgi complex through Rabex-5-mediated endocytosis.

Factors internalized by ligand-mediated endosome formation are believed to undergo lysosomal degradation, and ubiquitination is required for lysosomal sorting of many GTP-binding protein-coupled receptors.³⁸ Cells co-transfected with D_{2L}R-EGFP/PDGFR β or D_{2S}R-EGFP/PDGFR β were immunoprecipitated with anti-GFP antibody, and immunoprecipitates were analyzed with anti-ubiquitin antibody. Ubiquitination of both D₂R isoforms was unchanged after DA stimulation (Supplementary Figure 3b). Immunofluorescence also showed that most D_{2L}R/PDGFR β double-labeled vesicles do not overlap with lysosome compartments, as marked by the membrane protein 1 (LAMP-1; Supplementary Figure 3c).

Endocytotic activation of intracellular D_{2L}R is required for ERK activation in striatopallidal MSNs

We next monitored dynamics of quinpirole-mediated activation of PDGFR β and mitogen-activated protein kinase/ERK signaling in primary striatal neurons. Endogenous D₂R stimulation activates ERK in primary striatal neurons.¹⁰ Consistent with the previous observations, in primary striatal neurons isolated from WT mice, ERK phosphorylation increased significantly by 2.5-fold, peaking 10 min after quinpirole stimulation. Importantly, D₂R stimulation markedly stimulated PDGFR β tyrosine phosphorylation. In primary striatal neurons isolated from D_{2L}R-KO neurons, however, increased PDGFR β and ERK phosphorylation following quinpirole stimulation was not observed (Figure 4a). To investigate mechanisms underlying kinase activation, cultures of WT primary striatal neurons were pre-incubated with PTX, dynasore or a PDGFR inhibitor tyrphostin A9. As expected, all inhibitors completely blocked respective phosphorylation of PDGFR β and ERK following quinpirole stimulation. Similar results were obtained in cells transfected with Rabex-5 shRNA or pre-incubated with haloperidol (Figure 4b). We confirmed shRNA efficacy on Rabex-5 knockdown by immunoblotting of endogenous Rabex-5 protein in primary striatal neurons (Supplementary Figure 5a).

Next, we evaluated quinpirole-induced pERK immunoreactivity in cells from acutely prepared striatal slices labeled with the striatopallidal MSN marker preproenkephalin (ppEnk).³⁹ The

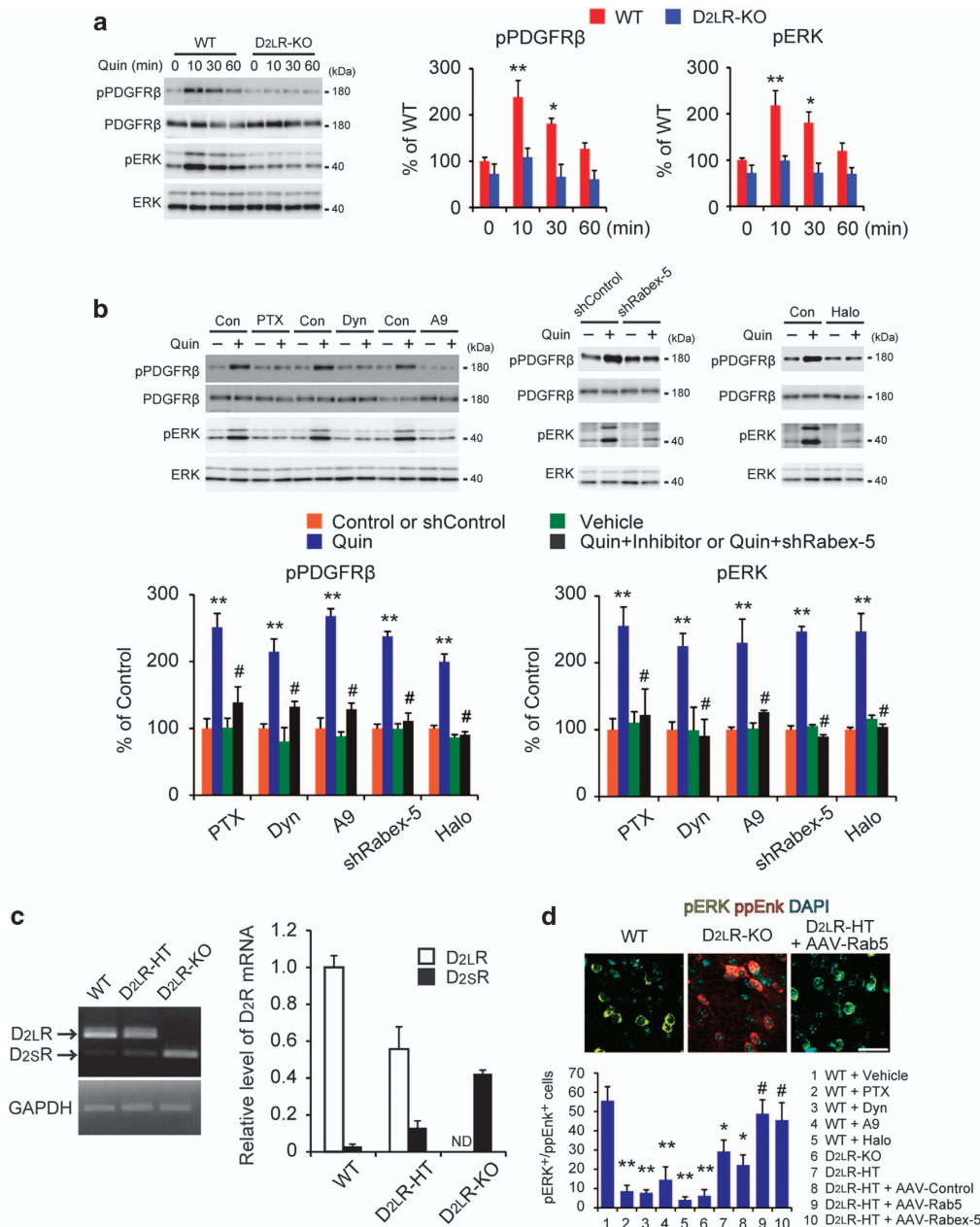


Figure 4. Endocytotic activation of intracellular D₂ receptor (D₂R) long isoform (D_{2L}R) is required for extracellular signal-regulated kinase (ERK) activation in striatopallidal medium spiny neurons (MSNs). **(a)** Left) Representative immunoblots of lysates made from primary striatal neurons incubated for indicated times with 10 μ M quinirole (Quin) and probed with indicated antibodies. (Right) Quantitative densitometry analyses. $**P < 0.01$, $*P < 0.05$ by two-way analysis of variance (ANOVA) with *post hoc* Tukey test. $n = 4$ per experiment. Three experiments were analyzed. **(b)** Representative immunoblots probed with indicated antibodies made from lysates from primary striatal neurons treated for 10 min with 10 μ M Quin. Striatal neurons were pre-incubated with 200 ng ml⁻¹ pertussis toxin (PTX), 80 μ M dynasore (Dyn), 10 μ M tyrphostin A9 (A9) or 10 μ M haloperidol (Halo) before 10 μ M Quin stimulation (top); quantitative densitometry analyses are shown at bottom. $**P < 0.01$ vehicle versus Quin, $\#P < 0.05$ Quin versus Quin plus indicated inhibitor by one-way ANOVA with *post hoc* Tukey test. $n = 4$ per experiment. Three experiments were analyzed. **(c)** Left) Representative agarose gel electrophoresis showing indicated reverse transcriptase–polymerase chain reaction (RT-PCR) products from mouse striatum. (Right) Semi-quantification of expression of D₂R mRNA isoforms ($n = 3$). ND, not detected. **(d)** Top) Representative confocal microscopy images showing double-staining of tissues in striatal slices for phospho- (p)ERK (extracellular signal-regulated kinase; green) and anti-preproenkephalin (ppEnk; red) following Quin stimulation. Nuclear DNA is labeled with 4,6-diamidino-2-phenylindole (DAPI; cyan). Scale bars, 30 μ m. (Bottom) Quantitative analyses of the number of pERK/ppEnk double-positive cells in slices. Striatal slices were pre-incubated with 200 ng ml⁻¹ PTX, 80 μ M Dyn, 10 μ M A9 or 10 μ M Halo before 10 μ M Quin stimulation $*P < 0.05$, $**P < 0.01$ versus wild type (WT)+vehicle, $\#P < 0.05$ versus D_{2L}R-HT+AAV-Control by one-way ANOVA with *post hoc* Tukey test. pERK/ppEnk double-positive cells were counted in four areas (350 \times 350 μ m²/area) per section of the dorsal striatum (6 sections per mouse, 3 mice per condition).

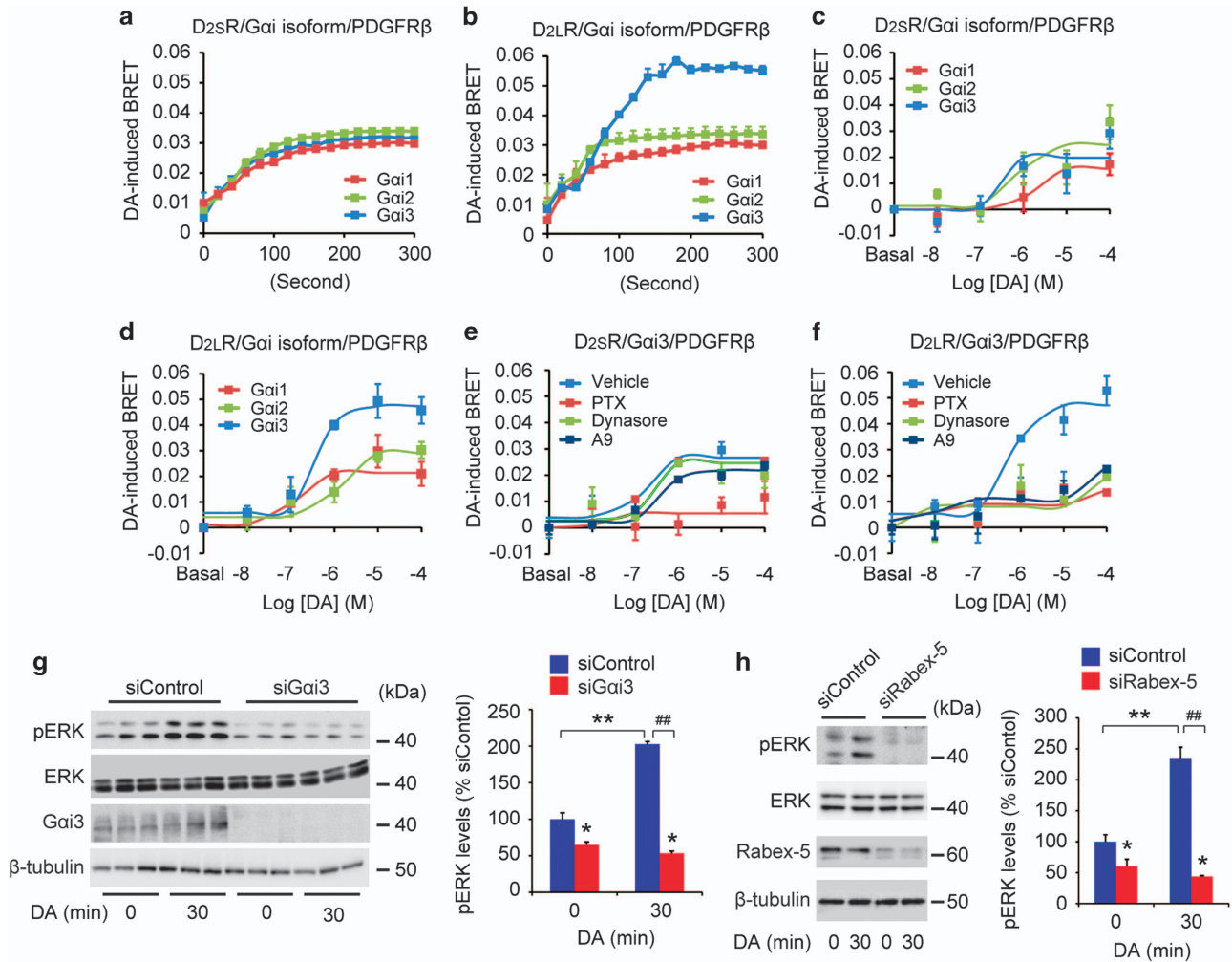


Figure 5. Interaction of D₂ receptor (D₂R) and Gai isoforms based on bioluminescence resonance energy transfer (BRET) analysis (**a, b**) Real-time measurement of BRET signals in HEK293T cells expressing RLuc8-tagged D₂R isoforms, wild type (WT)-platelet-derived growth factor receptor-β (PDGFRβ) and mVenus-tagged Gai isoforms in the presence of 10 μM DA. Three independent experiments performed in duplicate. Summary data are presented in Table 1. (**c, d**) Dose–response analysis of BRET signals in HEK293T cells expressing RLuc8-tagged D₂R isoforms, WT-PDGFRβ and mVenus-tagged Gai isoforms in the presence of indicated DA concentrations. Three independent experiments performed in duplicate. Summary data are presented in Table 2. (**e, f**) Dose–response analysis of BRET signals in HEK293T cells expressing RLuc8-tagged D₂R isoforms, WT-PDGFRβ and mVenus-tagged Gai isoforms. Cells were pretreated with 200 ng ml⁻¹ pertussis toxin (PTX), 80 μM dynasore, 10 μM typhostin A9 (A9) or 10 μM haloperidol (Halo) before the addition of substrate. Three independent experiments performed in duplicate. Summary data are presented in Table 3. (**g, h**; Left) Representative immunoblots probed with various antibodies and made from lysates of cells co-transfected with Gai3 (**g**) or Rabex-5 (**h**) short interfering RNA (siRNA), D₂R long isoform (D₂L) and PDGFRβ 30 min after 10 μM DA treatment. (Right) Quantitative densitometry analyses are shown. ***P* < 0.01, **P* < 0.05 versus 0 min in siControl, ##*P* < 0.01 versus 30 min with DA in siControl by one-way analysis of variance (ANOVA) with *post hoc* Tukey test, *n* = 3 each. Three independent experiments performed.

number of pERK/ppEnk double-positive neurons significantly decreased in WT slices pre-incubated with PTX, dynasore, typhostin A9 or haloperidol. Likewise, the number of pERK/ppEnk double-positive neurons also decreased in D₂L-R-KO compared with WT slices following quinpirole stimulation. The striatum of D₂L-R heterozygous knockout (D₂L-R-HT) mice, which exhibits a 50–60% reduction in D₂L-R mRNA levels based on RT-PCR analysis (Figure 4c) exhibited decreased numbers of pERK/ppEnk double-positive neurons. The number of pERK/ppEnk double-positive neurons in D₂L-R-HT was restored to levels seen in WT mouse striatum after bilateral intrastriatal injection of AAV-Rab5 to experimentally stimulate endocytosis^{40–42} or AAV-Rabex-5 without change in that of AAV-Control-injected D₂L-R-HT mice (Figure 4d). Taken together, our observations suggest that D₂L-R-induced PDGFRβ transactivation requires endocytotic activation of PTX-sensitive Gi proteins in striatopallidal MSNs.

Gai3 mediates intracellular D₂L-R signaling

To identify Gai isoforms required to activate D₂L-R signaling, we evaluated interactions of D₂L-R with Gai isoforms using a BRET-based receptor/G protein assay in HEK293T cells. Cells were transiently transfected with an energy donor, *Renilla Luciferase 8* (RLuc8)-tagged D₂R isoforms (D₂L-R-RLuc8 or D₂S-R-RLuc8), an acceptor in the form of mVenus-tagged Gai isoforms (Gai1-mVenus, Gai2-mVenus or Gai3-mVenus)²⁶ and WT-PDGFRβ. We first determined the kinetics of D₂R/Gai associations after agonist stimulation using real-time BRET measurements. In cells expressing D₂L-R-RLuc8/Gai3-mVenus/PDGFRβ, 10 μM DA treatment significantly increased BRET signals relative to other groups (Figure 5a and b and Table 1). Dose/response analysis using five different DA concentrations (0.01, 0.1, 1, 10 and 100 μM) revealed substantially elevated BRET signals in DA-treated cells expressing D₂L-R-RLuc8/Gai3-mVenus/PDGFRβ compared with other

constructs (Figure 5c and d and Table 2), and that activity was blocked by PTX. Moreover, dynasore or tyrphostin A9 completely abolished BRET signals in D_{2L}R-RLuc8/Gai3-mVenus/PDGFRβ-transfected cells but not in D_{2S}R-RLuc8/Gai3-mVenus/PDGFRβ-transfected cells (Figure 5e and f and Table 3). Similar results were obtained in cells transfected with Rabex-5 siRNA in D_{2L}R-RLuc8/Gai3-mVenus/PDGFRβ-transfected cells (Supplementary Figure 4a). We tested whether tyrphostin A9-mediated inhibition of PDGFRβ prevents the DA-induced association of D_{2L}R with Gai3 in D_{2L}R-RLuc8/Gai3-mVenus-transfected cells without PDGFRβ. As expected, the association of D_{2L}R with Gai3 significantly decreased compared with PDGFRβ-co-transfected cells, and it

could not be inhibited by treatment with tyrphostin A9 (Supplementary Figure 4b and 4c). We also confirmed the clear dose-dependent inhibitory action of other inhibitors including haloperidol (Supplementary Figure 4c). Immunocytochemical analysis revealed predominant expression of Gai1-mVenus and Gai2-mVenus in the plasma membrane, whereas Gai3-mVenus was localized in both the plasma membrane and Golgi apparatus as has been reported,⁴³ where it co-localized with D_{2L}R in an intracellular compartment (Supplementary Figure 4d). DA-induced ERK activation also significantly increased in Gai3-mVenus samples relative to other groups (Supplementary Figure 4e). In addition, ERK phosphorylation was completely inhibited by treatment of D_{2L}R/PDGFRβ-co-transfected cells with Gai3 or Rabex-5 siRNA (Figure 5g and h). To confirm the interaction with Gai3 and D_{2L}R/Rabex-5/PDGFRβ protein complex, we performed immunoprecipitation of cell extracts with an anti-Gai3 antibody followed by immunoblotting with anti-D₂R, anti-Rabex-5 or PDGFRβ antibody. These signals were present in HEK293T cells co-transfected with D_{2L}R/Gai3/PDGFRβ constructs (Supplementary Figure 4f) and mouse striatal extracts (Supplementary Figure 4g). Taken together, we conclude that DA-induced internalization of D_{2L}R/PDGFRβ-containing endosomes triggers an association of these proteins with intracellular Gai3 at the Golgi apparatus, eliciting ERK activation.

Intracellular D_{2L}R signaling is required for dendritic spine formation in striatal neurons

To assess whether ERK signal with the D_{2L}R exerts long-term effects on neural structure and function, we performed analysis of synaptic morphology and electrophysiology in primary culture of striatal neurons with mesencephalic DA neurons at DIV21. In

Table 1. BRET signal kinetics recorded over 5 min for each condition and showed as the BRET signal at the peak obtained in cells stimulated with 10 μM DA

| Receptor | Gai protein | BRET signal |
|-------------------|-------------|---------------------------------|
| D _{2S} R | Gai1 | 0.030 ± 0.11 × 10 ⁻³ |
| | Gai2 | 0.034 ± 0.48 × 10 ⁻³ |
| | Gai3 | 0.033 ± 0.94 × 10 ⁻³ |
| D _{2L} R | Gai1 | 0.031 ± 0.89 × 10 ⁻³ |
| | Gai2 | 0.034 ± 1.3 × 10 ⁻³ |
| | Gai3 | 0.058 ± 1.0 × 10 ^{-3a} |

Abbreviations: ANOVA, analysis of variance; BRET, bioluminescence resonance energy transfer; D_{2L}R, D₂ receptor long isoform; D_{2S}R, D₂ receptor short isoform. Data are presented as mean ± s.e.m. Three independent experiments performed with duplicate samples. ^a*P* < 0.01 (two-way repeated ANOVA with Tukey's post-test).

Table 2. Dose–response analysis of BRET signal in HEK293T cells expressing RLuc8-tagged D₂R isoforms/mVenus-tagged Gai isoforms in the presence of the indicated DA concentrations

| Receptor | Gai protein | BRET signal | EC ₅₀ (M) |
|-------------------|-------------|----------------------------------|---|
| D _{2S} R | Gai1 | 0.016 ± 1.76 × 10 ⁻³ | 0.26 × 10 ⁻⁶ ± 1.75 × 10 ⁻⁶ |
| | Gai2 | 0.025 ± 8.65 × 10 ⁻³ | 0.99 × 10 ⁻⁶ ± 0.42 × 10 ⁻⁶ |
| | Gai3 | 0.020 ± 9.30 × 10 ⁻³ | 2.33 × 10 ⁻⁶ ± 0.21 × 10 ⁻⁶ |
| D _{2L} R | Gai1 | 0.030 ± 8.95 × 10 ⁻³ | 3.10 × 10 ⁻⁶ ± 0.15 × 10 ⁻⁶ |
| | Gai2 | 0.031 ± 2.46 × 10 ⁻³ | 3.88 × 10 ⁻⁶ ± 0.90 × 10 ⁻⁶ |
| | Gai3 | 0.058 ± 2.54 × 10 ^{-3a} | 2.85 × 10 ⁻⁶ ± 0.35 × 10 ⁻⁶ |

Abbreviations: ANOVA, analysis of variance; BRET, bioluminescence resonance energy transfer; D_{2L}R, D₂ receptor long isoform; D_{2S}R, D₂ receptor short isoform. Data are presented as mean ± s.e.m. Three independent experiments performed with duplicate samples. ^a*P* < 0.01 (two-way repeated ANOVA with Tukey's post-test).

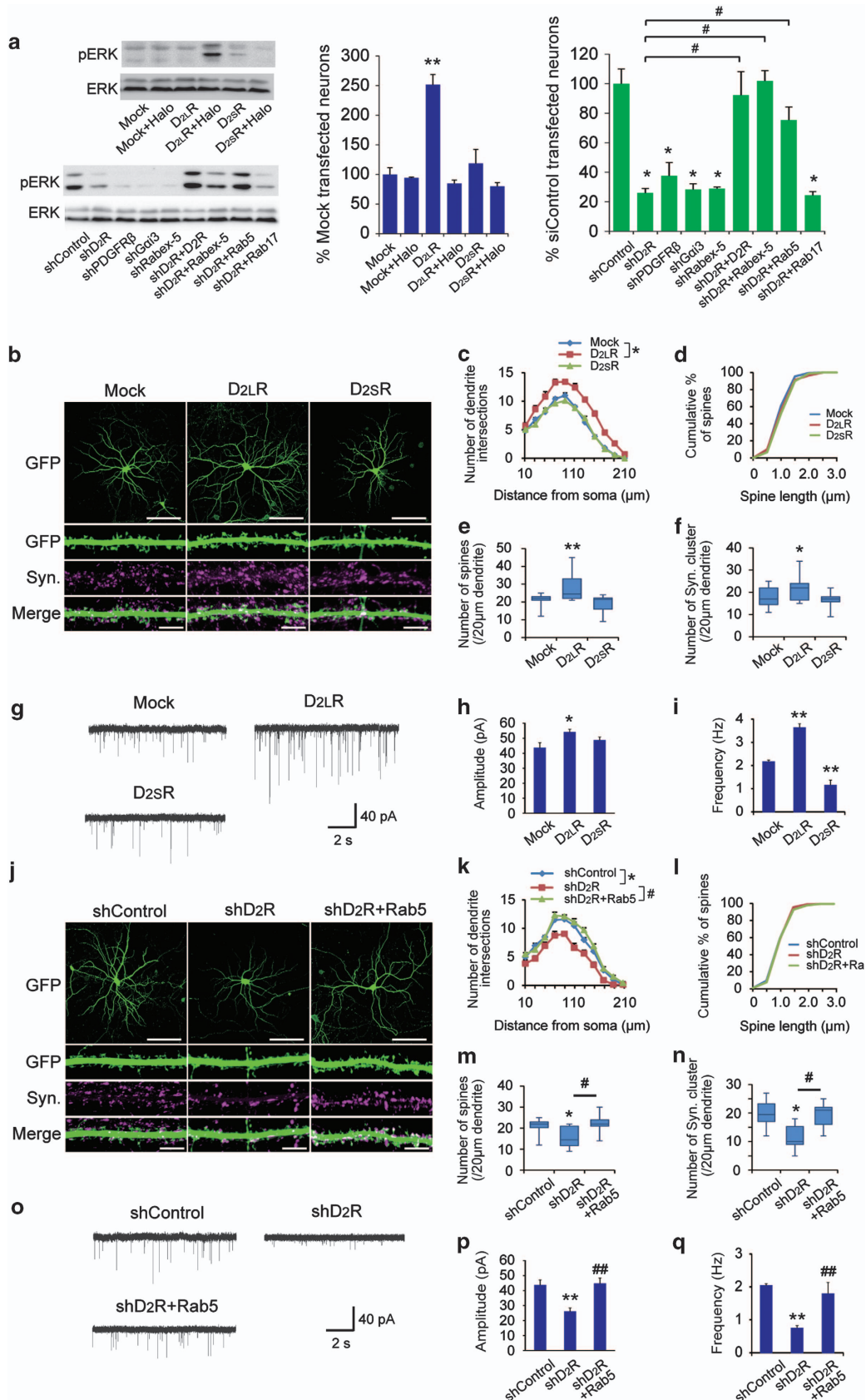
Table 3. Dose–response analysis of BRET signal in HEK293T cells expressing RLuc8-tagged D₂R isoforms/mVenus-tagged Gai3

| Receptor | Gai protein | Treatment | BRET signal | EC ₅₀ (M) |
|-------------------|-------------|---------------|----------------------------------|---|
| D _{2S} R | Gai3 | Vehicle | 0.027 ± 1.29 × 10 ⁻³ | 3.44 × 10 ⁻⁶ ± 0.54 × 10 ⁻⁶ |
| | | PTX | 0.005 ± 6.12 × 10 ^{-3a} | 2.51 × 10 ⁻⁵ ± 4.70 × 10 ⁻⁶ |
| | | Dynasore | 0.025 ± 4.80 × 10 ⁻³ | 3.29 × 10 ⁻⁶ ± 0.31 × 10 ⁻⁶ |
| | | Tyrphostin A9 | 0.022 ± 1.97 × 10 ⁻³ | 2.34 × 10 ⁻⁶ ± 0.29 × 10 ⁻⁶ |
| D _{2L} R | Gai3 | Vehicle | 0.047 ± 5.64 × 10 ⁻³ | 2.09 × 10 ⁻⁶ ± 0.14 × 10 ⁻⁶ |
| | | PTX | 0.014 ± 1.02 × 10 ^{-3b} | 3.05 × 10 ⁻⁵ ± 0.37 × 10 ⁻⁶ |
| | | Dynasore | 0.019 ± 0.10 × 10 ^{-3b} | 4.91 × 10 ⁻⁵ ± 6.21 × 10 ⁻⁶ |
| | | Tyrphostin A9 | 0.023 ± 0.83 × 10 ^{-3c} | 2.66 × 10 ⁻⁵ ± 9.21 × 10 ⁻⁶ |

Abbreviations: ANOVA, analysis of variance; BRET, bioluminescence resonance energy transfer; D_{2L}R, D₂ receptor long isoform; D_{2S}R, D₂ receptor short isoform; PTX, pertussis toxin. Data are presented as mean ± s.e.m. Three independent experiments performed with duplicate samples. D_{2S}R/Gai3, ^a*P* < 0.01 in the D_{2S}R/Gai3 group (two-way repeated ANOVA with Tukey's post-test); D_{2L}R/Gai3, ^b*P* < 0.01, ^c*P* < 0.05 in the D_{2L}R/Gai3 group (two-way repeated ANOVA with Tukey's post-test).

neurons transfected with D₂L_R at DIV0, ERK phosphorylation was significantly increased compared with mock and D₂S_R-expressed neurons. As expected, ERK phosphorylation significantly

decreased in neurons expressing shD₂R, shPDGFR β , shGai3 or shRabex-5. We confirmed shRNA efficacy against these shRNA plasmids by immunoblotting of endogenous mouse



proteins in cultured striatal neurons (Supplementary Figure 5a). Notably, ERK phosphorylation was recovered in neurons coexpressing shD₂R/D₂R, shD₂R/Rabex-5 and shD₂R/Rab5 (Figure 6a). Previous report showed that Rabex-5 activates at least two distinct Rabs, Rab5 and Rab17.²³ However, ERK phosphorylation was not recovered in neurons coexpressing shD₂R/Rab17, indicating that Rab5, but not Rab17, is involved in ERK signal with D₂R.

ERK signaling elicits changes in synaptic morphology, including neuronal dendritic spine formation.⁴⁴ To investigate D₂L₁R function in this process, we labeled cultured striatal neurons from WT mice by co-transfection with EGFP and either empty vector (mock), D₂L₁R or D₂S₁R constructs. Subsequently, striatal neurons at DIV21 were fixed and stained with anti-GFP and their dendritic spine morphology assessed. D₂L₁R overexpression significantly increased the number of dendritic branch intersections and spine/protrusion density without changing spine length relative to control cells transfected with EGFP alone, whereas D₂S₁R overexpression did not promote this change (Figure 6b–e). Consistently, D₂L₁R overexpression increased immunoreactivity of the presynaptic marker Syn, which was present in puncta along dendritic protrusions (Figure 6f). To determine whether synaptic activity accompanies these alterations, we examined sEPSCs. Consistent with increased spine density, D₂L₁R overexpression promoted significantly increased sEPSC amplitude and frequency. D₂S₁R overexpression significantly reduced in sEPSC frequency but had no effect on amplitude (Figure 6g–i).

Next, we asked whether shRNA-mediated knockdown of endogenous D₂R altered synaptic morphology. D₂R-knockdown neurons showed significantly decreased numbers of dendritic branch intersections and protrusion density compared with control shRNA-transfected neurons, without changes in spine/protrusion morphology (Figure 6j–m). Morphological alterations seen in D₂R-knockdown neurons were associated with reduced numbers of Syn-positive puncta (Figure 6n). Accordingly, D₂R knockdown significantly decreased sEPSC amplitude and frequency (Figure 6o–q). Similar results were seen in terms of spine morphology that PDGFR β , Rabex-5 or Gai3 knockdown neurons showed reduced number of dendritic branch intersections, spines and Syn-positive puncta (Supplementary Figure 5b–d). Moreover, D₂R or Rab5, but not Rab17, overexpression plus transfection with D₂R shRNA restored striatal neuron synapse formation, as estimated by the number of dendritic branch intersections and accumulation of Syn-positive puncta representing spines (Figure 6j–q and Supplementary Figure 5b–d), indicating that endocytotic D₂L₁R signaling is necessary for correct dendritic spine structure and synaptic activity in striatal neurons.

Intracellular D₂L₁R is essential for dendritic spine morphogenesis in striatopallidal MSNs *in vivo*

Next, we assessed the effect of intracellular D₂L₁R signaling *in vivo* using intracellular LY labeling methods. To distinguish striatonigral

from striatopallidal MSNs, we stained fixed striatal slices with ppEnk and DAPI. LY, ppEnk and DAPI fluorescence can be visualized simultaneously under ultraviolet excitation using a fluorescein long-pass filter, and it is possible to inject LY into specific striatopallidal MSNs (Figure 7a). LY-injected striatopallidal MSNs of the dorsal striatum showed significantly reduced numbers of dendritic branch intersections and decreased density of spines/protrusion in D₂L₁R-KO and D₂L₁R-HT relative to D₂L₁R-WT mice (Figure 7b–e) but no statistically significant changes in spine length (Figure 7f). Consistent with *in vitro* findings (Figure 6), AAV-Rab5 infection of the striatum partly rescued spine density phenotypes observed in AAV-Control-injected D₂L₁R-HT mice without altering dendritic arborization (Figure 7b–f). In LY-injected ppEnk-negative striatonigral MSNs of the dorsal striatum, there were no changes in numbers of dendritic branch intersections and density of spines/protrusion between D₂L₁R-WT and D₂L₁R-KO mice (Supplementary Figure 6a–d). Next, we evaluated dendritic spine morphogenesis following quinpirole stimulation in acutely prepared striatal slices. In WT mouse slices, spine density in LY-injected striatopallidal MSNs of the dorsal striatum significantly increased by 1h after quinpirole treatment, but comparable, statistically significant changes were not seen in D₂L₁R-KO slices (Figure 7g and h). Quinpirole treatment had no effect on the number of dendritic branch intersections or spine length in either genotype (data not shown). Taken together, *in vivo* analysis confirmed that D₂L₁R signaling in striatopallidal MSNs mediates in part dendritic spine morphogenesis.

Endocytotic activation of intracellular D₂L₁R is critical for haloperidol-induced cataleptic behavior

DA-stimulated ERK activity in the striatum is critical for synaptic and behavioral sensitization.⁴⁵ To determine whether novel intracellular D₂L₁R signaling described here mediates effects of typical antipsychotic drugs, we examined haloperidol-induced catalepsy behavior, which is significantly reduced in D₂L₁R-KO mice^{21,46} (Figure 8b). Specifically, we asked whether haloperidol treatment induces D₂R-mediated cataleptic behavior in central nervous system-specific PDGFR β cKO mice. As expected, cataleptic behavior was absent in PDGFR β cKO mice, as it is in D₂L₁R-KO mice (Figure 8c). D₂L₁R-HT mice showed approximately half of the cataleptic response seen in WT mice. When AAV-Rab5-IRES-EGFP was injected bilaterally into the striatum of D₂L₁R-HT mice (Figure 8a) and catalepsy analyzed 4 weeks later, the duration of catalepsy in injected animals was significantly greater than that in un-injected mice (Figure 8b). We verified that GFP fluorescence is comparable between cells transduced by AAV-EGFP and AAV-Rab5-IRES-EGFP in striatum (Supplementary Figure 7a), and AAV-EGFP-injected D₂L₁R-HT mice did not show alterations in cataleptic time in un-injected D₂L₁R-HT mice (Supplementary Figure 7b). In addition, all genotypes showed quinpirole-induced suppression of locomotor activity, which are reportedly mediated by presynaptic D₂R activity⁴⁶ (Supplementary Figure

Figure 6. D₂ receptor (D₂R) long isoform (D₂L₁R) signaling is required for dendritic spine formation and activity of cultured striatal neurons. **(a)** Left) Representative immunoblots of lysates made from primary striatal neurons transfected for indicated plasmids and probed with indicated antibodies. (Right) Quantitative densitometry analyses. *******P* < 0.01, ******P* < 0.05 versus mock or shControl, **#***P* < 0.05 versus shD₂R-transfected neurons by two-way analysis of variance (ANOVA) with *post hoc* Tukey test. *n* = 3 per experiment. Three experiments were analyzed. **(b, j)** Representative images of cultured striatal neurons co-transfected with EGFP and indicated plasmids. Neurons are double-stained for anti-GFP (green) and anti-synaptophysin (Syn; magenta). Scale bars, top panels; 100 μ m; bottom panels, 5 μ m. **(c, k)** The number of dendritic branch intersections. ******P* < 0.05 versus mock or shControl, **#***P* < 0.05 versus shD₂R by two-way ANOVA with *post hoc* Tukey test; *n* = 10 cells each. Three experiments were analyzed. **(d, l)** Relationship of cumulative percentage of spines to spine length. *P* > 0.05 by Kolmogorov–Smirnov test. Three experiments were analyzed. **(e, m)** Data were showed spine number of spines per 20 μ m dendrite. ******P* < 0.05, *******P* < 0.01 versus mock or shControl, **#***P* < 0.05 versus shD₂R by one-way ANOVA with *post hoc* Tukey test; *n* = 20 cells each. Three experiments were analyzed. **(f, n)** Number of spines showing Syn-positive puncta. ******P* < 0.05 versus mock or shControl, **#***P* < 0.05 versus shD₂R by one-way ANOVA with *post hoc* Tukey test; *n* = 20 cells each. Three experiments were analyzed. **(g–i, o–q)** Representative spontaneous excitatory postsynaptic current (sEPSC) data **(g, o)**, amplitude **(h, p)** and frequency **(i, q)** in cultured striatal neurons. *******P* < 0.01, ******P* < 0.05 versus mock or shControl, *******P* < 0.01 versus shD₂R-transfected neurons by one-way ANOVA with *post hoc* Tukey test; *n* = 5–6 cells. Three experiments were analyzed.

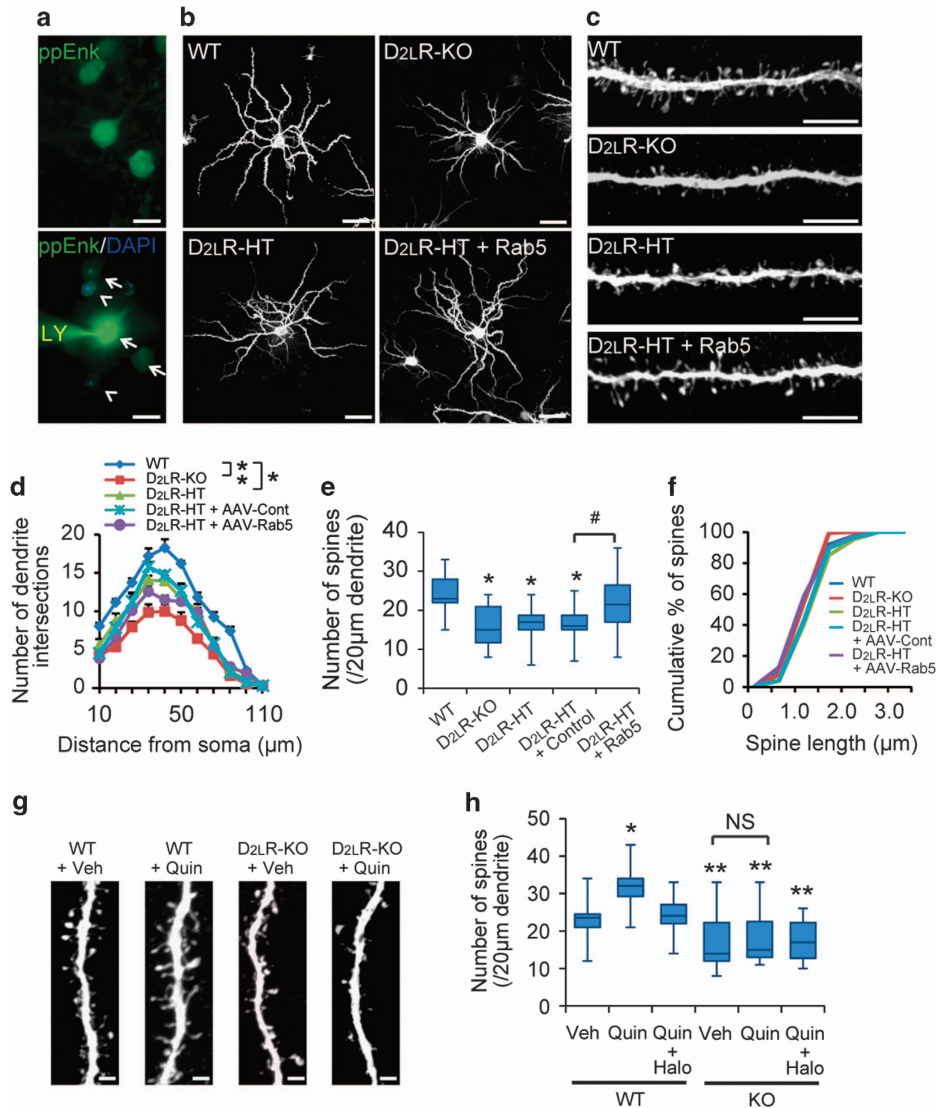


Figure 7. D₂ receptor (D₂R) long isoform (D₂L) is required for dendritic spine morphogenesis in striatopallidal medium spiny neuron (MSNs) *in vivo*. **(a)** Field view of dorsal striatum showing lucifer yellow (LY)-injected neurons (yellow), anti-preproenkephalin (ppEnk) staining (green) and nuclear 4,6-diamidino-2-phenylindole (DAPI; blue) under ultraviolet (UV) excitation using a fluorescein long-pass filter. Arrows, ppEnk-positive cells; arrowheads, ppEnk-negative cells. The bottom image (long-pass) shows the same field as the top image (FITC) a different filter. Scale bar, 10 μ m. **(b–c)** Low-magnification images of entire neurons **(b)** and dendritic spine morphology **(c)** in LY-injected ppEnk-positive cells. Scale bars, **(b)**, 100 μ m **(c)**, 5 μ m. **(d)** D₂L knockout (D₂L-R-KO) and D₂L-R-HT (Halo-tagged) mice show significantly decreased numbers of dendritic branch intersections compared with D₂L-R-wild type (WT) mice. ** $P < 0.01$ * $P < 0.05$ versus D₂L-R-WT by one-way analysis of variance (ANOVA) with *post hoc* Tukey test; $n = 10$ cells, $n = 3$ mice each. **(e)** D₂L-R-KO and D₂L-R-HT mice show significantly decreased spine numbers, whereas D₂L-R-HT+Rab5 animals show rescued spine numbers. * $P < 0.05$ versus D₂L-R-WT, # $P < 0.05$ versus D₂L-R-HT+AAV-Control by one-way ANOVA with *post hoc* Tukey test; $n = 20$ cells, $n = 3$ mice each. **(f)** Relationship of cumulative percentage of spines to spine length. $P > 0.05$ by Kolmogorov–Smirnov test. **(g)** Images showing morphology of dendritic spines in LY-injected ppEnk-positive neurons following quinpirole stimulation in acutely prepared striatal slices. Scale bars, 1 μ m. **(h)** WT slices show significantly increased spine number by 1 h after quinpirole treatment. ** $P < 0.01$, * $P < 0.05$ versus WT by one-way ANOVA with *post hoc* Tukey test; $n = 20$ cells, $n = 3$ mice each. NS, not significant.

7c and d). To determine whether novel D₂L signaling modulates D₁R function, we assessed catalepsy induced by SCH23390, a D₁R antagonist. SCH23390-induced catalepsy did not differ significantly in any genotype analyzed (Supplementary Figure 7e and f), indicating that D₂L signaling described here does not perturb D₁R function.

Immunohistochemical analysis indicates that PDGFR β is predominantly expressed in adult mouse neurons.²⁰ To determine PDGFR β localization in striatum, we double-stained with PDGFR β and cell-specific marker antibodies. Strong PDGFR β immunoreactivity was detected in cAMP-regulated phosphoprotein of 32 kDa

(DARPP-32)-positive cells, a marker of MSNs (Figure 8d). As expected, PDGFR β was localized both to D₁R- (Figure 8e) and D₂R-positive (Figure 8f) MSNs. PDGFR β immunoreactivity did not overlap with that of VGLUT1, a marker of glutamatergic terminals (Figure 8g) or tyrosine hydroxylase, a marker of dopaminergic neurons (Figure 8h). We also assessed the association between PDGFR β and D₁R or D₂R using antibodies to these factors in conjunction with dual recognition PLA. *In situ* PLA has been employed to test interaction of two proteins localized at distances of < 40 nm.⁴⁷ We observed clear PLA signals indicative of a PDGFR β interaction with D₂R in striatal sections. By contrast, PLA signals suggesting PDGFR β /D₁R

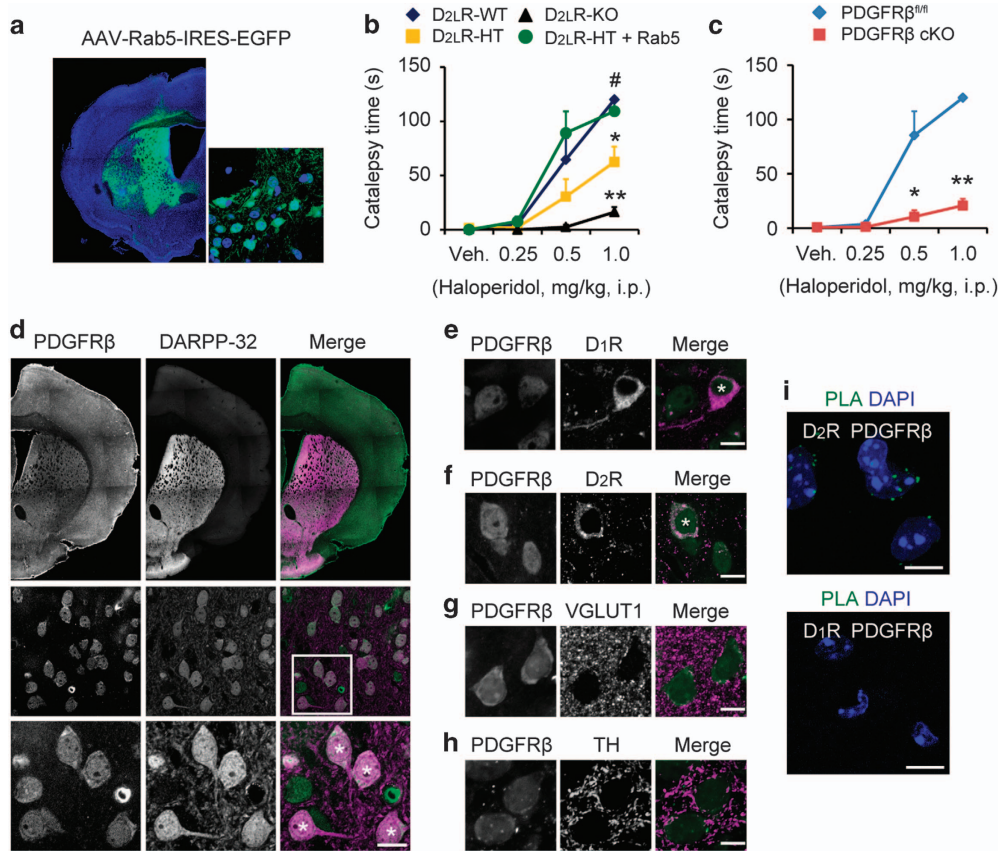


Figure 8. Endocytotic activation of intracellular D₂R long isoform (D₂L_R) is critical for haloperidol-induced cataleptic behavior. **(a)** Representative immunofluorescence image showing AAV-Rab5-IRES-EGFP expression in striatum. Blue, 4,6-diamidino-2-phenylindole (DAPI). Right panel: higher magnification of dorsal striatum. **(b)** Haloperidol-induced cataleptic time of AAV-Rab5-IRES-EGFP-injected D₂L_R-HT (Halo-tagged; D₂L_R-HT+Rab5) mice was significantly rescued comparable to levels seen in intact D₂L_R-wild type (WT) mice. D₂L_R-WT versus D₂L_R-knockout (D₂L_R-KO), genotype \times dose in catalepsy time ($F_{(3,48)} = 22.9, P < 0.01$). $^{**}P < 0.01$ by two-way analysis of variance (ANOVA) with *post hoc* Tukey test; $n = 7$ each. D₂L_R-WT versus D₂L_R-HT, genotype \times dose in catalepsy time ($F_{(3,48)} = 3.5, P < 0.05$). $^{*}P < 0.05$ by two-way ANOVA with *post hoc* Tukey test; $n = 7$ each. D₂L_R-HT versus D₂L_R-HT+Rab5, genotype \times dose in catalepsy time ($F_{(3,48)} = 3.6, P < 0.05$). $^{#}P < 0.05$ by two-way ANOVA with *post hoc* Tukey test; $n = 7$ each. **(c)** Haloperidol-induced catalepsy is not seen in central nervous system (CNS)-specific platelet-derived growth factor receptor- β (PDGFR β) conditional knockout (PDGFR β cKO) mice relative to PDGFR β floxed (PDGFR $\beta^{fl/fl}$) controls. PDGFR $\beta^{fl/fl}$ versus PDGFR β cKO, genotype \times dose in catalepsy time ($F_{(3,32)} = 18.1, P < 0.01$). $^{*}P < 0.05, ^{**}P < 0.01$ by two-way ANOVA with *post hoc* Tukey test; $n = 5$ each. **(d–h)** Confocal images showing localization of PDGFR β (green) with DARPP-32, D₁R, D₂ receptor (D₂R) or the presynaptic markers VGLUT1 and tyrosine hydroxylase (TH; magenta) in dorsal striatum. PDGFR β and DARPP-32 immunoreactivities almost completely merge **(d)**. PDGFR β was localized both to D₁R- **(e)** and D₂R-positive **(f)** medium spiny neurons (MSNs). PDGFR β immunoreactivity did not overlap with that of VGLUT1 **(g)** or TH **(h)**. Lower panels in **d** are high-magnification images. Scale bars, 10 μ m. White asterisks mark double-positive cells. **(i)** PDGFR β association with D₁R or D₂R as assessed by dual recognition proximity ligation *in situ* assay (PLA) with indicated antibodies. Signals indicating PDGFR β /D₂R interaction are clearly identified. PDGFR β /D₁R interaction is undetectable.

interaction were undetectable (Figure 8i). There was no background observed for the negative control without primary antibody (data not shown). These results suggest that PDGFR β protein co-localizes with D₂R but not D₁R in MSNs.

DISCUSSION

Here, we believe we provide the first evidence that Rabex-5/Rab5-dependent D₂L_R endocytosis accounts for dendritic spine formation in striatopallidum MSNs and that PDGFR β transactivation is critical for D₂L_R-mediated motor coordination through the striatum. D₂L_R is widely recognized as being expressed on the plasma membrane, where it couples with G_i protein in a manner similar to D_{2S}R. However, we found that after DA stimulation, D₂L_R- and PDGFR β -containing vesicles are transported by endocytosis to the Golgi complex, where D₂L_R transactivates PDGFR β through Gai3, enhancing ERK signaling. ERK activation likely triggers

downstream changes in synaptic plasticity, including alterations in dendritic spine formation (Figure 9).

Rabex-5 functions with Rabaptin-5 to activate Rab5, promoting early-endosome fusion.³⁴ Crystal structure analysis reveals that Rabex-5 CC domain binds loosely to Rab5-GDP-binding site to weakly inhibit GEF catalytic activity in the core domain. Binding of Rabaptin-5 to Rabex-5 CC domain perturbs interaction of the latter with the GEF inhibitory domain, exposing Rab5-GDP-binding site and partially enabling GEF activity. At the same time, the Rabex-5/Rabaptin-5 complex is recruited to early endosomes via binding of Rabaptin-5 C terminus to Rab5-GTP, further inducing conformational changes in Rabex-5/Rabaptin-5 complex and fully exposing the catalytic domain to Rab5-GDP to promote early-endosome fusion.^{34,48} We propose that D₂L_R stimulation promotes Rabex-5-induced GEF activity. Although mechanisms underlying this interaction remain unclear, DA-induced conformational changes in the D₂L_R/Rabex-5 complex may relieve auto-inhibitory activity

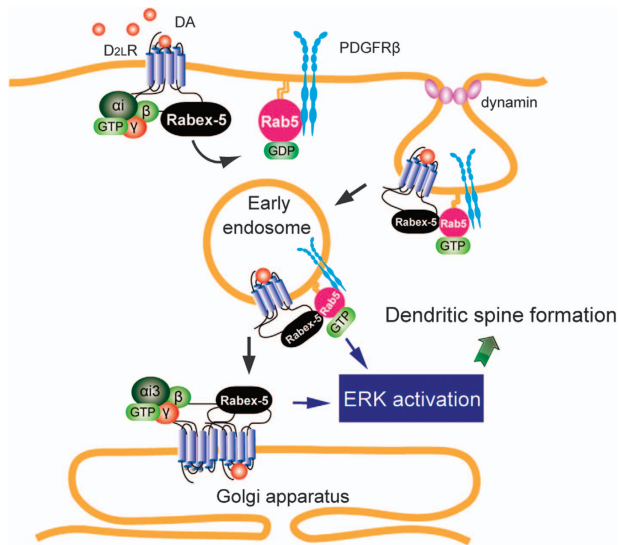


Figure 9. Schematic diagram showing D₂ receptor long isoform (D₂L_R) signaling events. D₂L_R-mediated Rabex-5 activation increases Rab5-GTP recruitment of early endosomal autoantigen 1 (EEA1), which promotes endocytosis of D₂L_R- and platelet-derived growth factor receptor- β (PDGFR β)-containing early endosomes through the clathrin-mediated pathway. Following dopamine (DA) stimulation, D₂L_R- and PDGFR β -containing early endosomes are transported to the Golgi complex, activating G α i3 and extracellular signal-regulated kinase (ERK). ERK activation likely triggers downstream effects, including dendritic spine formation.

of the Rabex-5 CC domain, thereby increasing its affinity to Rab5 and promoting exchange of GDP to GTP-bound form of Rab5.

The conventional model of D₂R signaling proposes that the receptor couples with G_i only in the plasma membrane.⁸ Therefore, DA-induced endocytosis has been believed to regulate D₂R activity, including desensitization and receptor downregulation or degradation.⁸ Notably, some studies report that persistent GTP-binding protein-coupled receptor signaling continues after internalization. In DA receptor signaling, DA or the D₁R agonist SKF81297 induces rapid D₁R internalization into early endosomes in association with G_s and consequent adenylyl cyclase activation. Additional cyclic AMP is produced in early-endocytotic membrane compartments.⁴⁹ In addition, thyroid-stimulating hormone (TSH) binds to the TSH receptor (TSHR) coupled to G_s, and TSH and TSHR complexes are internalized into perinuclear Golgi components associated with G α s and adenylyl cyclase to maintain cAMP production.⁵⁰ In G_i-coupled receptor signaling, binding of phosphorylated FTY720, an immunomodulator, to the sphingosine-1-phosphate receptor 1 maintains G_i-mediated signaling after internalization, leading to persistent adenylyl cyclase inhibition.⁵¹ Trimeric G proteins are also detected on membranes surrounding intracellular compartments, including the Golgi apparatus, in many mammalian tissues.⁵² Taken together, several GTP-binding protein-coupled receptors plus their ligands are internalized to regulate adenylyl cyclase activity in endosomes or intracellular Golgi compartments.

Here, we found that a G_i-coupled receptor, D₂L_R, is internalized to enhance ERK activity after DA stimulation. Evidence suggests that G_i-coupled receptor-mediated ERK activation is (i) dependent on PTX-sensitive G_i proteins that are independent of adenylyl cyclase inhibition,⁵³ (ii) dependent on G β γ subunits⁵⁴ and (iii) dependent on transactivation of receptor tyrosine kinases.⁵⁵ Although D₂R-mediated ERK activation through PDGFR β has been reported in Chinese hamster ovary cells,¹⁶ the physiological function of ERK activation in neurons following D₂L_R stimulation

remains unclear. Here, we have defined a critical upstream molecule, Rabex-5, as functioning in prolonged, D₂L_R-mediated ERK signaling. Rab5-GTP interacts with and activates PI3Ks, hVps34 and PI3K β .⁵⁶ PI3Ks mediate production of phosphatidylinositol 3-phosphate (PI(3)P) on early endosomes and recruitment of a set of PI(3)P-binding Rab5 effectors, including EEA1.⁵⁷ PI3K activation also induces PDGFR β internalization. Internalized PDGFR β reportedly remains phosphorylated and active, and principal components of phosphorylated ERK have been found in association with endosomes.⁵⁸ In future study, we will demonstrate whether ERK activation through the D₂L_R/Rabex-5 pathway is mediated by PI3K activation.

Consistent with previous reports,^{10,11} we observed significant increases in ERK phosphorylation in striatal primary culture and in striatal slices treated with quinpirole. However, some studies using *Drd1*- and *Drd2*-EGFP BAC-transgenic mice defined that basal ERK elevation is never observed in D₂R-expressing MSNs.^{59,60} In addition, D₂R stimulation by quinpirole inhibited basal ERK phosphorylation in D₁R-expressing MSNs, indicating that inhibition of DA release through activation of D₂ autoreceptor functions in basal ERK activation.⁶⁰⁻⁶² The striatal microcircuit is composed of MSNs that receive the excitatory corticostriatal glutamatergic innervation⁶³ and synapse with cholinergic interneuron terminals⁶⁴ as well as dopaminergic nigrostriatal fibers. D₂R is also present on corticostriatal terminals and cholinergic interneurons, and its stimulation inhibits both acetylcholine⁶⁵ and glutamate⁶⁶⁻⁶⁸ release from those terminals. Likewise, inhibition of ERK phosphorylation by quinpirole administration *in vivo* elicits diverse presynaptic modulation of dopaminergic, cholinergic and glutamatergic inputs in the striatum. For example, quinpirole-induced decreases in glutamate release are elicited by activation of presynaptic D₂Rs on glutamatergic terminals in mouse corticostriatal slices.⁶⁸ D₂R-KO mice exhibit reduced cocaine-induced behavioral sensitization with concomitant facilitation of glutamate release at corticostriatal synapses.^{69,70} D₂R activation by quinpirole also reduces synaptic inputs to striatal cholinergic interneurons in rat corticostriatal slices.⁶⁵ Therefore, further experiments are required to reveal the physiological relevance of striatal ERK activity stimulated by intracellular D₂L_R/PDGFR β signaling to functional connectivity of the basal ganglia circuitry, including corticostriatal and cholinergic synaptic transmission *in vivo*.

This study shows that increased ERK phosphorylation through intracellular D₂L_R in part alters dendritic spine morphogenesis in striatopallidal MSNs. Others have suggested that ERK-mediated morphological changes are regulated by phosphorylation of the synaptic protein synapsin I,⁷¹ translation of dendritic mRNAs⁷² and/or transcription of genes related to synaptic remodeling.⁷³ Decreased dendritic spine density selectively seen in striatopallidal MSNs has been reported in rodents following DA depletion by treatment with reserpine or 6-hydroxydopamine.⁷⁴ Indeed, striatal DA deficiency promotes a significant decrease in the number of MSN dendritic spines in Parkinson's disease patients.⁷⁵ Here, we confirm that D₂L_R-KO mice show significantly reduced MSN dendritic spine density. Rab5 overexpression rescued these phenotypes in striatopallidal MSNs. Thus, impaired intracellular D₂L_R signaling may underlie striatal neuron spine loss in Parkinson's disease patients.

In conclusion, we demonstrate ERK activation by PDGFR β transactivation after Rabex-5/Rab5-dependent D₂L_R internalization. Rabex-5-mediated ERK activation in endosomes or Golgi apparatus is critical for dendritic spine formation of striatopallidal MSNs. Further studies are required to define targets of Rabex-5/Rab5-mediated ERK activation that drive morphological changes seen in spines and dendrites of striatopallidal MSNs.

CONFLICT OF INTEREST

The authors declare no conflict of interest.

ACKNOWLEDGMENTS

We thank Dr Mitsunori Fukuda (Tohoku University, Sendai, Japan) for kindly providing Rabex-5, Rabex-5-D313A, Rabex-5C, Rabex-5C-D313A and Rabex-5 shRNA plasmids; Dr Wei-Xing Zong (Stony Brook University, Stony Brook, NY, USA) for kindly providing Rab5(WT), Rab5(S34N) and Rab5(Q79L) plasmids; Dr Guangpu Li (University of Oklahoma Health Sciences Center, Oklahoma City, OK, USA) for kindly providing GST-R5BD; and Dr Jonathan A. Javitch (Columbia University, New York, NY, USA) for kindly providing D_{2L}R-RLuc8, D₂₅R-RLuc8, Gai1-mVenus, Gai2-mVenus and Gai3-mVenus plasmids. This work was supported by Grants-in-Aid for Scientific Research on Innovative Area "Foundation of Synapse and Neurocircuit Pathology" from the Ministry of Education, Culture, Sports, Science and Technology, Japan (25110705 and 25460090 to NS) and (24102505 and 25293124 to KF).

REFERENCES

- Missale C, Nash R, Robinson SW, Jaber M, Caron MG. Dopamine receptors from structure to function. *Physiol Rev* 1998; **78**: 189–225.
- Seeman P, Lee T, Chau-wong M, Wong K. Antipsychotic drug doses and neuroleptic/dopamine receptors. *Nature* 1976; **261**: 717–719.
- Schizophrenia Working Group of the Psychiatric Genomics Consortium. Biological insights from 108 schizophrenia-associated genetic loci. *Nature* 2014; **511**: 421–427.
- Tan EK, Khajavi M, Thornby JI, Nagamitsu S, Jankovic J, Ashizawa T. Variability and validity of polymorphism association studies in Parkinson's disease. *Neurology* 2000; **55**: 533–538.
- Dal Toso R, Sommer B, Ewert M, Herb A, Pritchett DB, Bach A *et al*. The dopamine D2 receptor: two molecular forms generated by alternative splicing. *EMBO J* 1989; **8**: 4025–4034.
- Fetsko LA, Xu R, Wang Y. Effects of age and dopamine D2L receptor-deficiency on motor and learning functions. *Neurobiol Aging* 2005; **26**: 521–530.
- Zhang Y, Bertolino A, Fazio L, Blasi G, Rampino A, Romano R *et al*. Polymorphisms in human dopamine D2 receptor gene affect gene expression, splicing, and neuronal activity during working memory. *Proc Natl Acad Sci USA* 2007; **104**: 20552–20557.
- Beaulieu JM, Gainetdinov RR. The physiology, signaling, and pharmacology of dopamine receptors. *Pharmacol Rev* 2011; **63**: 182–217.
- Beaulieu JM, Sotnikova TD, Marion S, Lefkowitz RJ, Gainetdinov RR, Caron MG. An Akt/beta-arrestin 2/PP2A signaling complex mediates dopaminergic neurotransmission and behavior. *Cell* 2005; **122**: 261–273.
- Brami-Cherrier K, Valjent E, Garcia M, Pagès C, Hipskind RA, Caboche J. Dopamine induces a PI3-kinase-independent activation of Akt in striatal neurons: a new route to cAMP response element-binding protein phosphorylation. *J Neurosci* 2002; **22**: 8911–8921.
- Yan Z, Feng J, Fienberg AA, Greengard P. D(2) dopamine receptors induce mitogen-activated protein kinase and cAMP response element-binding protein phosphorylation in neurons. *Proc Natl Acad Sci USA* 1999; **96**: 11607–11612.
- Luo Y, Kokkonen GC, Wang X, Neve KA, Roth GS. D2 dopamine receptors stimulate mitogenesis through pertussis toxin-sensitive G proteins and Ras-involved ERK and SAP/JNK pathways in rat C6-D2L glioma cells. *J Neurochem* 1998; **71**: 980–990.
- Choi EY, Jeong D, Park KW, Baik JH. G protein mediated mitogen-activated protein kinase activation by two dopamine D2 receptors. *Biochem Biophys Res Commun* 1999; **256**: 33–40.
- Takeuchi Y, Fukunaga K. Differential regulation of NF-kappaB, SRE and CRE by dopamine D1 and D2 receptors in transfected NG108-15 cells. *J Neurochem* 2003; **85**: 729–739.
- Takeuchi Y, Fukunaga K. Different effects of five dopamine receptor subtypes on nuclear factor-kappaB activity in NG108-15 cells and mouse brain. *J Neurochem* 2004; **88**: 41–50.
- Oak JN, Lavine N, Van Tol HH. Dopamine D4 and D2L receptor stimulation of the mitogen-activated protein kinase pathway is dependent on trans-activation of the platelet-derived growth factor receptor. *Mol Pharmacol* 2001; **60**: 92–103.
- Kotecha SA, Oak JN, Jackson MF, Perez Y, Orser BA, Van Tol HH *et al*. A D2 class dopamine receptor transactivates a receptor tyrosine kinase to inhibit NMDA receptor transmission. *Neuron* 2002; **35**: 1111–1122.
- Beazely MA, Tong A, Wei WL, Van Tol H, Sidhu B, MacDonald JF. D2-class dopamine receptor inhibition of NMDA currents in prefrontal cortical neurons is platelet-derived growth factor receptor-dependent. *J Neurochem* 2006; **98**: 1657–1663.
- Horiuchi H, Lippé R, McBride HM, Rubino M, Woodman P, Stenmark H *et al*. A novel Rab5 GDP/GTP exchange factor complexed to Rabaptin-5 links nucleotide exchange to effector recruitment and function. *Cell* 1997; **90**: 1149–1159.
- Shioda N, Moriguchi S, Oya T, Ishii Y, Shen J, Matsushima T *et al*. Aberrant hippocampal spine morphology and impaired memory formation in neuronal platelet-derived growth factor β -receptor lacking mice. *Hippocampus* 2012; **22**: 1371–1378.
- Wang Y, Xu R, Sasaoka T, Tonegawa S, Kung MP, Sankoorikal EB. Dopamine D2 long receptor-deficient mice display alterations in striatum-dependent functions. *J Neurosci* 2000; **20**: 8305–8314.
- Yamaguchi H, Aiba A, Nakamura K, Nakao K, Sakagami H, Goto K *et al*. Dopamine D2 receptor plays a critical role in cell proliferation and proopiomelanocortin expression in the pituitary. *Genes Cells* 1996; **1**: 253–268.
- Mori Y, Matsui T, Fukuda M. Rabex-5 protein regulates dendritic localization of small GTPase Rab17 and neurite morphogenesis in hippocampal neurons. *J Biol Chem* 2013; **288**: 9835–9847.
- Wise A, Watson-Koken MA, Rees S, Lee M, Milligan G. Interactions of the α 2A-adrenoceptor with multiple Gi-family G-proteins: studies with pertussis toxin-resistant G-protein mutants. *Biochem J* 1997; **321**: 721–728.
- Shioda N, Yamamoto Y, Watanabe M, Binias B, Owada Y, Fukunaga K. Heart-type fatty acid binding protein regulates dopamine D2 receptor function in mouse brain. *J Neurosci* 2010; **30**: 3146–3155.
- Urizar E, Yano H, Kolster R, Galés C, Lambert N, Javitch JA. CODA-RET reveals functional selectivity as a result of GPCR heteromerization. *Nat Chem Biol* 2011; **7**: 624–630.
- Liu J, Lamb D, Chou MM, Li YJ, Li G. Nerve growth factor-mediated neurite outgrowth via regulation of Rab5. *Mol Biol Cell* 2007; **18**: 1375–1384.
- Manders EM, Verbeek FJ, Aten JA. Measurement of co-localization of objects in dual color confocal images. *J Microsc* 1993; **169**: 375–382.
- Shioda N, Beppu H, Fukuda T, Li E, Kitajima I, Fukunaga K. Aberrant calcium/calmodulin-dependent protein kinase II (CaMKII) activity is associated with abnormal dopamine D2 receptor morphology in the ATRX mutant mouse brain. *J Neurosci* 2011; **31**: 346–358.
- Roy A, Kucukural A, Zhang Y. I-TASSER: a unified platform for automated protein structure and function prediction. *Nat Protoc* 2010; **5**: 725–738.
- Lee S, Tsai YC, Mattera R, Smith WJ, Kostelansky MS, Weissman AM *et al*. Structural basis for ubiquitin recognition and autoubiquitination by Rabex-5. *Nat Struct Mol Biol* 2006; **13**: 264–271.
- Penengo L, Mapelli M, Murachelli AG, Confalonieri S, Magri L, Musacchio A *et al*. Crystal structure of the ubiquitin binding domains of rabex-5 reveals two modes of interaction with ubiquitin. *Cell* 2006; **124**: 1183–1195.
- Delprato A, Merithew E, Lambright DG. Structure, exchange determinants, and family-wide rab specificity of the tandem helical bundle and Vps9 domains of Rabex-5. *Cell* 2004; **118**: 607–617.
- Delprato A, Lambright DG. Structural basis for Rab GTPase activation by VPS9 domain exchange factors. *Nat Struct Mol Biol* 2007; **14**: 406–412.
- Takeuchi Y, Fukunaga K. Differential subcellular localization of two dopamine D2 receptor isoforms in transfected NG108-15 cells. *J Neurochem* 2003; **85**: 1064–1074.
- Bonifacino JS, Rojas R. Retrograde transport from endosomes to the trans-Golgi network. *Nat Rev Mol Cell Biol* 2006; **8**: 568–579.
- Christoforidis S, McBride HM, Burgoyne RD, Zerial M. The Rab5 effector EEA1 is a core component of endosome docking. *Nature* 1999; **397**: 621–625.
- Marchese A, Paing MM, Temple BR, Trejo JG. Protein-coupled receptor sorting to endosomes and lysosomes. *Annu Rev Pharmacol Toxicol* 2008; **48**: 601–629.
- Curran EJ, Watson SJ Jr. Dopamine receptor mRNA expression patterns by opioid peptide cells in the nucleus accumbens of the rat: a double *in situ* hybridization study. *J Comp Neurol* 1995; **361**: 57–76.
- Bucci C, Parton RG, Mather IH, Stunnenberg H, Simons K, Hoflack B, Zerial M. The small GTPase rab5 functions as a regulatory factor in the early endocytic pathway. *Cell* 1992; **70**: 715–728.
- Somsel Rodman J, Wandinger-Ness A. Rab GTPases coordinate endocytosis. *J Cell Sci* 2000; **113**: 183–192.
- Dou Z, Pan JA, Dbouk HA, Ballou LM, DeLeon JL, Fan Y *et al*. Class IA. PI3K p110 β subunit promotes autophagy through Rab5 small GTPase in response to growth factor limitation. *Mol Cell* 2013; **50**: 29–42.
- Le-Niculescu H, Niesman I, Fischer T, DeVries L, Farquhar MG. Identification and characterization of GIV, a novel Galpha *i/s*-interacting protein found on COPI, endoplasmic reticulum-Golgi transport vesicles. *J Biol Chem* 2005; **280**: 22012–22020.
- Zhai S, Ark ED, Parra-Bueno P, Yasuda R. Long-distance integration of nuclear ERK signaling triggered by activation of a few dendritic spines. *Science* 2013; **342**: 1107–1111.
- Shiflett MW, Balleine BW. Contributions of ERK signaling in the striatum to instrumental learning and performance. *Behav Brain Res* 2011; **218**: 240–247.

- 46 Usiello A, Baik JH, Roug -Pont F, Picetti R, Dierich A, LeMeur M *et al*. Distinct functions of the two isoforms of dopamine D2 receptors. *Nature* 2000; **408**: 199–203.
- 47 S derberg O, Gullberg M, Jarvius M, Ridderstr le K, Leuchowius KJ, Jarvius J *et al*. Direct observation of individual endogenous protein complexes *in situ* by proximity ligation. *Nat Methods* 2006; **3**: 995–1000.
- 48 Zhang Z, Zhang T, Wang S, Gong Z, Tang C, Chen J *et al*. Molecular mechanism for Rabex-5 GEF activation by Rabaptin-5. *Elife* 2014; **3**: e02687.
- 49 Kotowski SJ, Hopf FW, Seif T, Bonci A, von Zastrow M. Endocytosis promotes rapid dopaminergic signaling. *Neuron* 2011; **71**: 278–290.
- 50 Calebiro D, Nikolaev VO, Gagliani MC, de Filippis T, Dees C, Tacchetti C *et al*. Persistent cAMP-signals triggered by internalized G-protein-coupled receptors. *PLoS Biol* 2009; **7**: e1000172.
- 51 Mullershausen F, Zecri F, Cetin C, Billich A, Guerini D, Seuwen K. Persistent signaling induced by FTY720-phosphate is mediated by internalized S1P1 receptors. *Nat Chem Biol* 2009; **5**: 428–434.
- 52 Marrari Y, Crouthamel M, Irannejad R, Wedegaertner PB. Assembly and trafficking of heterotrimeric G proteins. *Biochemistry* 2007; **46**: 7665–7677.
- 53 Lajiness ME, Chio CL, Huff RM. D2 dopamine receptor stimulation of mitogenesis in transfected Chinese hamster ovary cells: relationship to dopamine stimulation of tyrosine phosphorylations. *J Pharmacol Exp Ther* 1993; **267**: 1573–1581.
- 54 van Biesen T, Hawes BE, Luttrell DK, Krueger KM, Touhara K, Porfiri E *et al*. Receptor-tyrosine-kinase- and G beta gamma-mediated MAP kinase activation by a common signalling pathway. *Nature* 1995; **376**: 781–784.
- 55 Shah BH, Catt KJ. GPCR-mediated transactivation of RTKs in the CNS: mechanisms and consequences. *Trends Neurosci* 2004; **27**: 48–53.
- 56 Shin HW, Hayashi M, Christoforidis S, Lacas-Gervais S, Hoepfner S, Wenk MR *et al*. An enzymatic cascade of Rab5 effectors regulates phosphoinositide turnover in the endocytic pathway. *J Cell Biol* 2005; **170**: 607–618.
- 57 Simonsen A, Lipp  R, Christoforidis S, Gaullier JM, Brech A, Callaghan J *et al*. EEA1 links PI(3)K function to Rab5 regulation of endosome fusion. *Nature* 1998; **394**: 494–498.
- 58 Waters CM, Connell MC, Pyne S, Pyne NJ. c-Src is involved in regulating signal transmission from PDGFbeta receptor-GPCR(s) complexes in mammalian cells. *Cell Signal* 2005; **17**: 263–277.
- 59 Bertran-Gonzalez J, Bosch C, Maroteaux M, Matamalas M, Herv  D, Valjent E *et al*. Opposing patterns of signaling activation in dopamine D1 and D2 receptor-expressing striatal neurons in response to cocaine and haloperidol. *J Neurosci* 2008; **28**: 5671–5685.
- 60 Gangarossa G, Perroy J, Valjent E. Combinatorial topography and cell-type specific regulation of the ERK pathway by dopaminergic agonists in the mouse striatum. *Brain Struct Funct* 2013; **218**: 405–419.
- 61 Mercuri NB, Saiardi A, Bonci A, Picetti R, Calabresi P, Bernardi G *et al*. Loss of autoreceptor function in dopaminergic neurons from dopamine D2 receptor deficient mice. *Neuroscience* 1997; **79**: 323–327.
- 62 Centonze D, Usiello A, Gubellini P, Pisani A, Borrelli E, Bernardi G *et al*. Dopamine D2 receptor-mediated inhibition of dopaminergic neurons in mice lacking D2L receptors. *Neuropsychopharmacology* 2002; **27**: 723–726.
- 63 Dub  L, Smith AD, Bolam JP. Identification of synaptic terminals of thalamic or cortical origin in contact with distinct medium-size spiny neurons in the rat neostriatum. *J Comp Neurol* 1988; **267**: 455–471.
- 64 Holt DJ, Graybiel AM, Saper CB. Neurochemical architecture of the human striatum. *J Comp Neurol* 1997; **384**: 1–25.
- 65 Pisani A, Bonsi P, Centonze D, Calabresi P, Bernardi G. Activation of D2-like dopamine receptors reduces synaptic inputs to striatal cholinergic interneurons. *J Neurosci* 2000; **20**: RC69.
- 66 Fisher RS, Levine MS, Sibley DR, Ariano MA. D2 dopamine receptor protein location: Golgi impregnation-gold toned and ultrastructural analysis of the rat neostriatum. *J Neurosci Res* 1994; **38**: 551–564.
- 67 Sesack SR, Aoki C, Pickel VM. Ultrastructural localization of D2 receptor-like immunoreactivity in midbrain dopamine neurons and their striatal targets. *J Neurosci* 1994; **14**: 88–106.
- 68 Bamford NS, Zhang H, Schmitz Y, Wu NP, Cepeda C, Levine MS *et al*. Heterosynaptic dopamine neurotransmission selects sets of corticostriatal terminals. *Neuron* 2004; **42**: 653–663.
- 69 Welter M, Vallone D, Samad TA, Meziane H, Usiello A, Borrelli E. Absence of dopamine D2 receptors unmasks an inhibitory control over the brain circuitries activated by cocaine. *Proc Natl Acad Sci USA* 2007; **104**: 6840–6845.
- 70 Cepeda C, Hurst RS, Altemus KL, Flores-Hern andez J, Calvert CR, Jokel ES *et al*. Facilitated glutamatergic transmission in the striatum of D2 dopamine receptor-deficient mice. *J Neurophysiol* 2001; **85**: 659–670.
- 71 Jovanovic JN, Benfenati F, Siow YL, Sihra TS, Sanghera JS, Pelech SL *et al*. Neurotrophins stimulate phosphorylation of synapsin I by MAP kinase and regulate synapsin I-actin interactions. *Proc Natl Acad Sci USA* 1996; **93**: 3679–3683.
- 72 Kelleher RJ 3rd, Govindarajan A, Jung HY, Kang H, Tonegawa S. Translational control by MAPK signaling in long-term synaptic plasticity and memory. *Cell* 2004; **116**: 467–479.
- 73 Thomas GM, Hagan RL. MAPK cascade signalling and synaptic plasticity. *Nat Rev Neurosci* 2004; **5**: 173–183.
- 74 Day M, Wang Z, Ding J, An X, Ingham CA, Shering AF *et al*. Selective elimination of glutamatergic synapses on striatopallidal neurons in Parkinson disease models. *Nat Neurosci* 2006; **9**: 251–259.
- 75 Villalba RM, Smith Y. Differential striatal spine pathology in Parkinson's disease and cocaine addiction: a key role of dopamine? *Neuroscience* 2013; **251**: 2–20.

Supplementary Information accompanies the paper on the Molecular Psychiatry website (<http://www.nature.com/mp>)